New Journal of Physics
The open-access journal for physics

# Radiation statistics in homogeneous isotropic turbulence

**C B da Silva[1], I Malico[2] and P J Coelho[1,3]**
[1] Mechanical Engineering Department, IDMEC/LAETA, Instituto Superior Técnico, Technical University of Lisbon, Av. Rovisco Pais, 1049-001 Lisboa, Portugal
[2] Physics Department, University of Évora, Rua Romão Ramalho, 59, 7000-671 Évora, Portugal
E-mail: carlos.silva@ist.utl.pt, imbm@uevora.pt and pedro.coelho@ist.utl.pt

*New Journal of Physics* **11** (2009) 093001 (34pp)
Received 28 May 2009
Published 2 September 2009
Online at http://www.njp.org/
doi:10.1088/1367-2630/11/9/093001

**Abstract.** An analysis of turbulence–radiation interaction (TRI) in statistically stationary (forced) homogeneous and isotropic turbulence is presented. A direct numerical simulation code was used to generate instantaneous turbulent scalar fields, and the radiative transfer equation (RTE) was solved to provide statistical data relevant in TRI. The radiation intensity is non-Gaussian and is not spatially correlated with any of the other turbulence or radiation quantities. Its power spectrum exhibits a power-law region with a slope steeper than the classical $-5/3$ law. The moments of the radiation intensity, Planck-mean and incident-mean absorption coefficients, and emission and absorption TRI correlations are calculated. The influence of the optical thickness of the medium, mean and variance of the temperature and variance of the molar fraction of the absorbing species is studied. Predictions obtained from the time-averaged RTE are also included. It was found that while turbulence yields an increase of the mean blackbody radiation intensity, it causes a decrease of the time-averaged Planck-mean absorption coefficient. The absorption coefficient self-correlation is small in comparison with the temperature self-correlation, and the role of TRI in radiative emission is more important than in radiative absorption. The absorption coefficient–radiation intensity correlation is small, which supports the optically thin fluctuation approximation, and justifies the good predictions often achieved using the time-averaged RTE.

[3] Author to whom any correspondence should be addressed.

## Contents



## 1. Introduction

Most flows of practical relevance are turbulent. In some of them, radiative heat transfer plays an important role, e.g. in most combustion systems (furnaces, boilers, engines, etc) and in fire. It was found several decades ago that there is an interaction between turbulence and thermal radiation, i.e. turbulence influences thermal radiation and vice versa. As an example, the heat flux incident on a surface and coming from a radiative source at a given mean temperature depends on the temperature fluctuations rather than just on the mean temperature. Presently, it is widely accepted that this interaction yields a significant increase of the radiative heat fluxes in comparison with laminar flows [1, 2]. It has been reported that turbulence–radiation interaction (TRI) may enhance mean radiation levels by more than 100% in comparison with estimates based on mean scalar properties, i.e. mean temperature and molar fraction of chemical species (see e.g. [3]). The main reason for this phenomenon is the strong nonlinearity between the radiative emission and temperature. However, our knowledge about TRI is still limited. As a consequence, TRI is often ignored in numerical simulations or accounted for by assuming that it is only due to the influence of temperature fluctuations on the emissive power of the medium.

Thermal radiative transfer is generally calculated using the radiative transfer equation (RTE). For a non-scattering medium, this equation expresses the variation of the radiation intensity along an elementary optical path as the difference between emission and absorption of radiation along that path, as outlined in section 2.4. The emission is proportional to the blackbody radiation intensity, while the absorption is proportional to the radiation intensity. The proportionality factor for both emission and absorption is the absorption coefficient of the medium, which physically represents the inverse of the average distance travelled by a photon until it is absorbed in the medium.

An approach to account for TRI in Reynolds-averaged Navier–Stokes (RANS) simulation of turbulent flows with radiative transfer consists in the solution of the time-averaged RTE with the mean radiation intensity as the dependent variable [1], [4]–[10]. Still, it is difficult to model the correlation between fluctuations of the radiation intensity and fluctuations of the absorption coefficient of the medium, which appears in the time-averaged form of the RTE. This correlation is generally ignored, assuming that the individual eddies are homogeneous, optically thin and statistically independent. This is the so-called optically thin fluctuation approximation (OTFA) [11], which has been used in most of RANS calculations that account for TRI. The error of this approximation is largely unknown. It has been claimed that the error introduced by this approximation is small, even if it does not hold for wavelengths in the vicinity of the centre of the most important absorption bands of radiatively participating gaseous species. A model has recently been proposed [12] to avoid the OTFA by approximating the correlation between fluctuations of the incident radiation and fluctuations of the absorption coefficient. It is based on the assumption that the diffusion approximation holds for optically thick eddies. However, only limited evaluation has been performed, particularly in the range where eddies are neither optically thick nor optically thin.

A powerful method to account for the TRI consists of the solution of the RTE for instantaneous values of scalars (temperature and species concentrations). This requires a sufficiently large number of solutions based on instantaneous scalar distributions to ensure statistically meaningful results. Moreover, the instantaneous scalar distributions are not available in RANS, and need to be generated in such a way that the mean values, variance and relevant spatial and temporal auto-correlations and cross-correlations are satisfied. Stochastic models for the generation of time series of scalar distributions have been developed for this purpose [3], [13]–[15]. The large number of realizations implied by the stochastic methods prevents their application to practical engineering calculations.

Most numerical studies dealing with TRI have been carried out in the framework of RANS. In fact, apart from the recent studies by Poitou *et al* [16], Coelho [17] and Roger *et al* [18], large eddy simulations generally neglect TRI [19, 20], even though there is no guarantee of the accuracy of this procedure.

Advances in computer power have allowed the direct numerical simulation (DNS) of the exact Navier–Stokes equations. Although DNS is a powerful tool to provide fundamental and reliable insight on turbulent flows, it can only be applied to simple geometries and low to moderate Reynolds number flows, because of the high computational requirements. Therefore, it cannot be used in present engineering calculations. Homogeneous isotropic turbulence consists in the simplest possible flow configuration, in which the Navier–Stokes equations are solved in a cubic domain with periodic boundary conditions in the three spatial directions. Instantaneous fields from DNS of isotropic turbulence show the existence of intense vorticity regions in the form of tubes ('worms') with radii and length of the order of the Kolmogorov and integral scales, respectively [21, 22]. DNS of isotropic turbulence has been used to study some detailed aspects of turbulence physics, and to develop and assess turbulence models. Moreover, some works used DNS of isotropic turbulence to study fundamental issues related to combustion, e.g. the analysis of flamelets in premixed turbulent combustion [23].

A theoretical study of the influence of thermal radiation on thermal turbulence spectra in the case of homogeneous and isotropic turbulence was presented in [24]. TRI in a homogeneously turbulent medium was reported in [14], but a stochastic model rather than DNS was used to generate the instantaneous scalar fields. Recently, DNS was used to investigate TRI in simple

premixed and diffusion combustion systems. Wu *et al* [25] investigated an idealized statistically one-dimensional (1D) turbulent premixed laminar flame. They found that the temperature self-correlation is the dominant contribution to TRI only for optically thin media, but even in this case, the absorption coefficient–Planck function and the absorption coefficient–intensity correlations are not negligible. All these correlations are significant at intermediate values of optical thickness. Deshmukh *et al* [26] studied a statistically homogeneous isotropic decaying turbulent non-premixed system, while Deshmukh *et al* [27] considered a statistically 1D decaying turbulent non-premixed system. The contributions from the three individual correlations mentioned above have been computed, and all of them have been found to be important in intermediate to large values of the optical thickness of the medium, although their relative contribution is a function of the optical thickness.

In the present study, the influence of the optical thickness, mean and variance of the temperature and the molar fraction of the radiatively participating species on radiation statistics and correlations is investigated in a homogeneous and isotropic turbulent medium. This follows a preliminary study [28] where statistical data of the radiation intensity field were reported for conditions typical of the region downstream of a turbulent jet diffusion flame where turbulence is approximately homogeneous. A classical pseudo-spectral code for the simulation of isotropic turbulence in non-reactive flows [29] is used, which allows the computation of forced and freely decaying isotropic turbulence by means of DNS of the full Navier–Stokes equations and the transport equation for a passive scalar.

Combustion is not considered in the present work, so that the instantaneous scalar field computed from DNS is used as input data for the radiative transfer calculations, i.e. the instantaneous fields of temperature and molar fraction of an absorbing species are determined from the transported scalar field, after prescribing the mean value and the variance of the temperature and of the molar fraction of the species. Then, these instantaneous scalar fields are used to solve the RTE, along a large number of lines of sight, in order to collect the statistical data. In the present work, there is no influence of the radiative transfer calculations on the DNS simulation, i.e. there is only a one-way coupling between turbulence and radiation. The goal here is to prepare the ground for future works where the effects of the turbulent statistics on the radiative properties of the medium will be thoroughly investigated.

A statistical narrow band model was used in [28] to calculate the radiative properties of the medium. However, some features of the radiative calculations reported in that work were not fully consistent with the requirements of the flow simulation, such as the definition of the boundary conditions, and the dependence of the statistical data on the number of samples was not investigated. These drawbacks are eliminated in the present work, which extends the analysis to the full spectrum rather than just one band, and examines the influence of several parameters on the radiation statistics and correlations. In addition, predictions obtained from the solution of the time-averaged form of the RTE are included.

It is worth to point out that the physical problem addressed in the present work, which consists of a homogeneous and isotropic turbulent medium that emits and absorbs thermal radiation, and with periodic boundary conditions, represents an idealized situation. It is interesting from a theoretical point of view, and may be approached, but not fully achieved, in some practical applications, e.g. in a perfectly stirred reactor. Accordingly, caution should be taken in the extrapolation of the results reported here to real physical problems and conditions.

## 2. Theoretical background

### *2.1. The Navier–Stokes equations and the spectra of turbulence*

In incompressible flows of a Newtonian fluid, whose kinematic viscosity $\nu$ and density $\rho$ are taken as constants, the fields of velocity $u_i$ and pressure $p$ are governed by the Navier–Stokes equations:

$$\frac{\partial u_i}{\partial t} + \frac{\partial (u_i u_j)}{\partial x_j} = -\frac{1}{\rho}\frac{\partial p}{\partial x_i} + \nu \frac{\partial^2 u_i}{\partial x_j \, \partial x_j}. \tag{1}$$

The velocity verifies an incompressible condition

$$\frac{\partial u_i}{\partial x_i} = 0. \tag{2}$$

In turbulent flows the nonlinear term on the left-hand side of equation (1) is dominant, and is responsible for the continuous amplification and transport of velocity fluctuations, while the molecular viscosity effects represented by the last term in (1) continually diffuse and dissipate the energy of the fluctuations. Turbulent flows are characterized by a wide range of interacting space and timescales in which most of the turbulent kinetic energy $u_i u_i/2$ is associated with the large scales, while the small scales are mainly responsible by the viscous dissipation of energy. The viscous dissipation rate is $\varepsilon = 2\,\nu\, S_{ij}\, S_{ij}$, where $S_{ij} = 0.5(\partial u_i/\partial x_j + \partial u_j/\partial x_i)$ is the rate-of-strain tensor. An interesting and intriguing feature of turbulent flows, for sufficiently high Reynolds number, is the fact that the dissipation rate $\varepsilon$ is independent of the viscosity. Indeed, the dissipation rate is completely dictated by the large scales of motion, while the small scales have to adjust their dynamics to the energy input from the large scales through the intensification of the local velocity gradients.

The 3D energy spectrum $E(k)$ describes the contribution of each wavenumber to the turbulent kinetic energy

$$\frac{u_i u_i}{2} = \int_0^\infty E(k)\mathrm{d}k. \tag{3}$$

For sufficiently high Reynolds numbers, Kolmogorov postulated the existence of an inertial range of scales where the kinetic energy from the large scales is passed down to the small scales. Assuming that these inertial scales are statistically isotropic, and are dictated only by the rate of energy transfer (which must balance the viscous dissipation rate), the energy spectrum for this range has the form

$$E(k) = C_\mathrm{k}\varepsilon^{2/3}k^{-5/3}, \tag{4}$$

where $C_\mathrm{k}$ is the Kolmogorov constant. This constant is close to $C_\mathrm{k} \approx 1.6$ [30].

A passive scalar field $\theta$, which is simply advected with the flow, is governed by a simple transport equation:

$$\frac{\partial \theta}{\partial t} + \frac{\partial (\theta u_j)}{\partial x_j} = \gamma \frac{\partial^2 \theta}{\partial x_j \partial x_j}, \tag{5}$$

**Table 1.** Details of the DNS. The Reynolds number $Re_\lambda$ is based on the Taylor micro-scale, $\nu$ is the molecular viscosity, $k_{\max}$ the maximum resolved wavenumber, $Sc$ the Schmidt number, $L_{11}$ the velocity integral scale, $\eta$ the Kolmogorov micro-scale and $\eta_B$ the Batchelor micro-scale.

| $Re_\lambda$ | $\nu$ | $Sc$ | $k_{\max}\eta$ | $k_{\max}\eta_B$ | $L_{11}$ | $\eta(\times 10^{-2})$ | $\eta_B(\times 10^{-2})$ |
|---|---|---|---|---|---|---|---|
| 95.6 | 0.006 | 0.7 | 1.8 | 2.1 | 1.24 | 2.8 | 3.3 |

where $\gamma$ is the scalar diffusivity. The scalar variance $\theta^2/2$ is associated with a scalar spectrum $E_\theta(k)$ through

$$\frac{\theta^2}{2} = \int_0^\infty E_\theta(k)\mathrm{d}k. \tag{6}$$

Assuming the existence of an inertial range for the scalar field in a situation where it is only advected by the velocity fluctuations—the *inertial-convective* range—the scalar spectrum is given by

$$E_\theta(k) = C_{CO}\varepsilon_\theta \varepsilon^{-1/3} k^{-5/3}, \tag{7}$$

where $C_{CO}$ is the Corrsin–Obukhov constant, $\varepsilon_\theta = \gamma G_j G_j$ is the scalar dissipation rate and $G_j = \partial\theta/\partial x_j$ is the scalar gradient. Typical values are close to $C_{CO} \approx 0.6$ [30].

### 2.2. DNS of homogeneous isotropic turbulence

The DNS data bank used in the present work consists in a statistically steady (forced) homogeneous isotropic turbulence simulation used by da Silva and Pereira [29, 31]. The simulations were carried out with a standard pseudo-spectral code in which the temporal advancement is made with an explicit 3rd order Runge–Kutta scheme. Details about the DNS solver may be found in [32]. The physical domain consists in a periodic box of side equal to $2\pi$ and using $N = 192$ collocation points in each spatial direction. Aliasing errors were removed using the 3/2 rule. Both the velocity and scalar fields were forced in order to sustain the turbulence using the method described in [33]. The forcing was imposed on three wavenumbers concentrated on $k_p = 3$, both for the velocity and for the scalar fields. It is designed to inject kinetic energy and scalar variance during the simulation at a rate that more or less balances the instantaneous viscous dissipation rate $\varepsilon$ and the scalar dissipation rate $\varepsilon_\theta$. Therefore, after an initial transient, the velocity and the passive scalar fields reach a state where they are statistically stationary and statistically equivalent. The forcing affects only a very small wavenumber region associated with the large scales of motion. As described in [31], it was checked that both the large and the small scales of motion comply with the strong resolution requirements needed in DNS: $L_{box} > 4L_{11}$, where $L_{box}$ is the size of the computational domain and $L_{11}$ is the integral scale of the velocity field, and $k_{\max}\eta > 1.5$ and $k_{\max}\eta_B > 1.5$, where $k_{\max}$ is the maximum resolved wavenumber, $\eta = (\nu^3/\varepsilon)^{1/4}$ and $\eta_B = Sc^{-1/2}\eta$ are the Kolmogorov and the Batchelor micro-scales, respectively, and $Sc$ is the Schmidt number. Thus, the size of the computational domain does not affect the largest flow structures, and a good resolution of the dissipative scales was ensured, following Pope [34]. Table 1 lists the physical and computational parameters

of the simulation. The data bank used here consists in 40 instantaneous passive scalar fields corresponding to a Schmidt number equal to $Sc = 0.7$. For this simulation, the Reynolds number based on the Taylor scale is $Re_\lambda = u_{\rm rms}\lambda/\nu = 95.6$, where $\lambda^2 = \langle u'^2\rangle/\langle(\partial u/\partial x)'^2\rangle$ is the Taylor micro-scale, $u_{\rm rms} = \langle u'^2\rangle^{1/2}$ is the root-mean-square (rms) of the velocity fluctuations, and $\nu$ is the kinematic viscosity. As shown in [31], velocity and scalar spectra display a $-5/3$ range, which shows the existence of an inertial range region. Therefore, this simulation is already representative of a high Reynolds number flow, i.e. it features the most important characteristics of turbulence, such as a dissipation rate independent from the viscosity and the Kolmogorov–Obukhov $-5/3$ inertial scaling law of the energy and scalar variance spectra. More details on this simulation are given in [31].

### *2.3. Framework of radiative transfer calculations*

The radiative transfer calculations were performed also using a cubic box. However, it is not convenient to take the side of this box equal to $2\pi$, as is the flow domain. In fact, in order to carry out the parametric study reported in section 3, it is useful to define the temperature and the chemical composition of the medium, from which the absorption coefficient is computed, independently from the optical thickness of the medium. The optical thickness is the integral of the absorption coefficient along the direction of propagation of radiation. In the present work, the medium is statistically homogeneous and isothermal, and its optical thickness is taken as the Planck-mean absorption coefficient in the absence of turbulent fluctuations multiplied by the length of the side of the cubic domain. Therefore, this length is not prescribed, but is instead determined from the selected optical thickness of the medium, temperature and molar fraction of the absorbing species.

The medium is assumed to be a mixture of $CO_2$ and radiatively transparent species, e.g. $N_2$. The temperature and the molar fraction of $CO_2$ were assumed to be fully correlated. Although this assumption is not strictly true, since the diffusion coefficient of $CO_2$ may be slightly different from the thermal diffusion coefficient, it is justified by the experimental data in many reactive flows, which reveal a strong correlation between the temperature and molar fraction of the species, and by the Burke–Schumann theory for diffusion flames [35]. It is also consistent with combustion models that relate the instantaneous thermochemical state of the gaseous mixture to a single scalar, typically mixture fraction, e.g. the laminar flamelet model [36]. Even though combustion is not considered in the present work, the properties of the medium are typical of those found downstream of the flame region in combustion systems. Hence, a single passive scalar transport equation is solved using DNS. The computed data for this passive scalar may be used to define the instantaneous fields of temperature and $CO_2$ molar fraction.

The instantaneous field of a passive scalar calculated in the DNS code must be rescaled into the radiation domain to provide the instantaneous fields of temperature and molar fraction of $CO_2$. To accomplish this goal, the mean and the variance of temperature and of the molar fraction of the absorbing species were prescribed in the radiative transfer simulations, and kinematic similarity was assumed. Therefore, the instantaneous temperature field used in the radiation computations, $T_{\rm rad}(\vec{x})$, was determined using the instantaneous temperature field from the DNS data, $T_{\rm DNS}(\vec{x})$, as follows:

$$T_{\rm rad}(\vec{x}) = \bar{T}_{\rm rad}(\vec{x}) + T_{\rm DNS}(\vec{x})\sqrt{\overline{T'^2_{\rm rad}}/\overline{T'^2_{\rm DNS}}}, \tag{8}$$

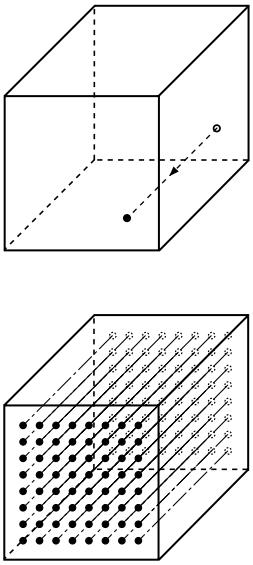

**Figure 1.** Equivalence between temporal and spatial statistics under homogeneous and isotropic turbulence.

where $\bar{T}_{\mathrm{rad}}(\vec{x})$ is the mean temperature at point $\vec{x}$, and $\overline{T'^2_{\mathrm{rad}}}$ and $\overline{T'^2_{\mathrm{DNS}}}$ are the variances of the temperature fields from the radiation and from the isotropic turbulence simulation, respectively. Similarly, the molar fraction of the absorbing species, $x_{\mathrm{CO_2}}$, is obtained as follows:

$$x_{\mathrm{CO_2,rad}}(\vec{x}) = \bar{x}_{\mathrm{CO_2,rad}}(\vec{x}) + x_{\mathrm{CO_2,DNS}}(\vec{x})\sqrt{\overline{x'^2_{\mathrm{CO_2,rad}}}/\overline{x'^2_{\mathrm{CO_2,DNS}}}}. \tag{9}$$

The radiative transfer calculations use these instantaneous fields as input data, and consist in the integration of the RTE along the lines of sight, followed by a statistical analysis of the results obtained. Under the conditions of statistically stationary, homogeneous and isotropic turbulence, an ergodic hypothesis is assumed, where spatial, temporal and ensemble averages are equivalent. Therefore, the statistical data computed from a time series of scalar data along a single optical path parallel to a coordinate axis are identical to the statistical data calculated from all optical paths parallel to the coordinate axes at a given time, as illustrated in figure 1. The statistical data reported in section 3 were obtained from the DNS data using all the available $192^2$ optical paths parallel to a coordinate axis, which are statistically indistinguishable. All the optical paths start from one of the six faces of the cubic domain and are normal to that face. This means that $6 \times 192^2 \times N_t \approx 2.2 \times 10^5 \times N_t$ samples are used to obtain the results described below, $N_t$ being the number of instantaneous fields considered.

### *2.4. Radiative transfer calculations*

The RTE for an emitting, absorbing and non-scattering medium may be written as [37]

$$\frac{\mathrm{d}I_\nu}{\mathrm{d}s} = -\kappa_\nu I_\nu + \kappa_\nu I_{\mathrm{b}\nu}, \tag{10}$$

where $I_\nu$ is the spectral radiation intensity, $I_{\mathrm{b}\nu}$ the spectral blackbody radiation intensity, $\kappa_\nu$ the spectral absorption coefficient and $s$ the coordinate along the direction of propagation of radiation. The subscript $\nu$ stands for the wavenumber. The governing equation for the total

radiation intensity may be expressed as

$$\frac{\mathrm{d}I}{\mathrm{d}s} = -\kappa_G I + \kappa_P I_\mathrm{b}, \tag{11}$$

where $I$ and $I_\mathrm{b}$ are the total radiation intensity and the total blackbody radiation intensity, obtained from integration of $I_\nu$ and $I_{\mathrm{b}\nu}$ over the whole spectrum, respectively. The total blackbody radiation intensity is proportional to the fourth power of temperature, the proportionality constant being the Stefan–Boltzmann constant. The Planck-mean and the incident-mean absorption coefficients, $\kappa_\mathrm{P}$ and $\kappa_G$ respectively, are defined as follows:

$$\kappa_P = \int_0^\infty \kappa_\nu I_{\mathrm{b}\nu}\mathrm{d}\nu \Big/ \int_0^\infty I_{\mathrm{b}\nu}\mathrm{d}\nu, \tag{12a}$$

$$\kappa_G = \int_0^\infty \kappa_\nu G_\nu \mathrm{d}\nu \Big/ \int_0^\infty G_\nu \mathrm{d}\nu, \tag{12b}$$

where $G_\nu$ is the spectral incident radiation, defined as the integral over all directions of the spectral radiation intensity. If the radiation intensity does not change with the direction, which is valid on a statistical basis in the case of a homogeneous and isotropic medium, as in the present work, different directions are statistically indistinguishable, and $\kappa_G$ may be expressed as

$$\kappa_G = \int_0^\infty \kappa_\nu I_\nu \mathrm{d}\nu \Big/ \int_0^\infty I_\nu \mathrm{d}\nu. \tag{13}$$

The following definitions have also been used in equation (11):

$$\kappa_P I_\mathrm{b} = \int_0^\infty \kappa_\nu I_{\mathrm{b}\nu}\mathrm{d}\nu, \tag{14a}$$

$$\kappa_G I = \int_0^\infty \kappa_\nu I_\nu \mathrm{d}\nu. \tag{14b}$$

Integration of equation (10) along a line of sight, in the case of a non-scattering medium, yields [37]

$$I_\nu(s) = I_\nu(0)\exp\left(-\int_0^s \kappa_\nu(s')\mathrm{d}s'\right) + \int_0^s I_{\mathrm{b}\nu}(s')\kappa_\nu(s')\exp\left(-\int_{s'}^s \kappa_\nu(s'')\mathrm{d}s''\right)\mathrm{d}s'. \tag{15}$$

As is usual in simulations of isotropic turbulence, periodic boundary conditions were used in the present DNS. Consistency between the DNS and the radiative transfer calculations requires that periodic boundary conditions should also be used in the radiative transfer calculations if the DNS data are taken as an input. Specifically, this periodic boundary condition requires that the radiation intensity entering the calculation domain at $s = 0$ is equal to the leaving intensity at $s = L$, $L$ being the length of the side of the cubic domain. Therefore, the medium is in radiative equilibrium and $I_\nu(L) = I_\nu(0)$ for any optical path parallel to the coordinate axes. Accordingly,

the radiation intensity entering the domain is calculated from this condition. Such a condition, which was also used in [26, 27], is actually found in real radiative transfer problems in the limit of a transparent medium or of a homogeneous and isothermal optically thick medium. It is also approximately found in well-stirred reactors.

The radiative properties of the medium were evaluated using the correlated $k$-distribution (CK) method [38]. The parameters of the CK method were taken from the tabulated data by Soufiani and Taine [39]. Hence, equation (15) is written as

$$I_{i,\Delta\nu_k}(s) = I_{i,\Delta\nu_k}(0)\exp\left[-\int_0^s k_{i,k}(s^*)\mathrm{d}s^*\right] + \int_0^s k_{i,k}(s^*)I_{\mathrm{b},\Delta\nu_k}(s^*)\exp\left[-\int_{s^*}^s k_{i,k}(s^{**})\mathrm{d}s^{**}\right]\mathrm{d}s^*, \tag{16}$$

where $k_{i,k}$ is the absorption coefficient associated with the $i$th quadrature point and the $k$th band, $I_{i,\Delta\nu_k}$ is the spectral radiation intensity integrated over the $k$th band for the $i$th quadrature point and $\Delta\nu_k$ is the $k$th wavenumber interval length. The periodic boundary condition is enforced by setting $I_{i,\Delta\nu_k}(L) = I_{i,\Delta\nu_k}(0)$. The total radiation intensity is calculated as

$$I = \sum_{k=1}^{N_\mathrm{b}}\sum_{i=1}^{N_\mathrm{Q}} \omega_i I_{i,\Delta\nu_k}, \tag{17}$$

where $\omega_i$ is the quadrature weight, $N_\mathrm{Q}$ the number of quadrature points and $N_\mathrm{b}$ the number of bands. The integrals in equation (16) were numerically evaluated using Simpson's rule, and the parameters of the CK method were interpolated from the tabulated data using cubic splines in order to keep the order of accuracy of the radiative calculations consistent with the order of accuracy of the DNS solver.

### 2.5. *Time-averaged form of the RTE*

The time-averaged form of equation (11), which needs to be solved in RANS, is given by

$$\frac{\mathrm{d}\bar{I}}{\mathrm{d}s} = -\bar{\kappa}_G\bar{I} - \overline{\kappa_G' I'} + \overline{\kappa_\mathrm{P} I_\mathrm{b}}. \tag{18}$$

The second term on the right-hand side of equation (18) is neglected if the OTFA is employed. In order to investigate the importance of TRI, it is useful to define the following diagnostic quantities:

$$R_{I_\mathrm{b}} = I_\mathrm{b}(\bar{T})/\,\bar{I}_\mathrm{b} = \bar{T}^4/\overline{T^4}, \tag{19a}$$

$$R_{\kappa_G} = \kappa_G\left(\bar{T}, \bar{x}_{\mathrm{CO}_2}\right)/\bar{\kappa}_G, \tag{19b}$$

$$R_{\kappa_\mathrm{P}} = \kappa_\mathrm{P}\left(\bar{T}, \bar{x}_{\mathrm{CO}_2}\right)/\bar{\kappa}_\mathrm{P}, \tag{19c}$$

$$R_{kI} = \bar{\kappa}_G\bar{I}/\overline{\kappa_G I}, \quad R^*_{kI} = 1 - R_{kI} = \overline{\kappa_G' I'}/\overline{\kappa_G I}, \tag{19d}$$

$$R_{kI_\mathrm{b}} = \bar{\kappa}_\mathrm{P}\bar{I}_\mathrm{b}/\overline{\kappa_\mathrm{P} I_\mathrm{b}}, \quad R^*_{kI_\mathrm{b}} = 1 - R_{kI_\mathrm{b}} = \overline{\kappa_\mathrm{P}' I_\mathrm{b}'}/\overline{\kappa_\mathrm{P} I_\mathrm{b}}, \tag{19e}$$

$$\rho_{kI} = \frac{\overline{\kappa_G' I'}}{\sqrt{\overline{\kappa_G'^2}\;\overline{I'^2}}}. \tag{19f}$$

The temperature self-correlation, which may also be defined as $\overline{T^4}/\bar{T}^4$, is quantified by $R_{I_\mathrm{b}}$, while the Planck-mean and incident-mean absorption coefficient self-correlations are quantified by $R_{k_P}$ and $R_{k_G}$, respectively. The relevance of the absorption coefficient–radiation intensity and absorption coefficient–temperature correlations are quantified by $R^*_{kI}$ (or $R_{kI}$) and $R^*_{kI_\mathrm{b}}$(or $R_{kI_\mathrm{b}}$), respectively.

### *2.6. Prediction of the radiation intensity and radiation statistics*

In the next section, the statistical results obtained from the solution of the RTE along a sufficiently large number of optical paths, using the instantaneous scalar data from DNS, are compared with the solution of the time-averaged form of the RTE. If the OTFA is employed and the CK model is used, the total time-averaged radiation intensity is computed as follows [8]:

$$\bar{I}(s)=\sum_k\sum_i \omega_i \bar{I}_{i,\Delta\nu_k}(s)=\sum_k\sum_i \omega_i\left[\bar{I}_{i,\Delta\nu_k}(0)\exp\left(-\bar{k}_{i,k}s\right)+\left(\overline{k_{i,k}I_{\mathrm{b},\Delta\nu_k}}\big/\bar{k}_{i,k}\right)\left(1-\exp\left(-\bar{k}_{i,k}\,s\right)\right)\right]. \tag{20}$$

The derivation of equation (20) requires that $\bar{k}_{i,k}$ does not change along the optical path between 0 and $s$, which is true in the present case, because the medium is statistically homogeneous.

A similar equation expressed in terms of the mean absorption coefficients, which will be useful for the discussion of results, is obtained from integration of equation (11) along a line of sight:

$$\bar{I}(s)=\bar{I}(0)\exp\left(-\bar{k}_G s\right)+\left(\overline{kI_\mathrm{b}}\big/\bar{k}_G\right)\left(1-\exp\left(-\bar{k}_G s\right)\right). \tag{21}$$

Since the medium is statistically homogeneous and the boundary conditions are periodic, equation (20) may be written as

$$\bar{I}(s)=\sum_k\sum_i \omega_i \bar{I}_{i,\Delta\nu_k}(s)=\sum_k\sum_i \omega_i\,\overline{k_{i,k}I_{\mathrm{b},\Delta\nu_k}}\big/\bar{k}_{i,k}, \tag{22}$$

and equation (21) is simplified as

$$\bar{I}(s)=\overline{kI_\mathrm{b}}\big/\bar{k}_G. \tag{23}$$

The mean values of the absorption coefficient and emission term may be estimated from integration of the instantaneous values of these quantities weighted by a probability density function (pdf). Here, it is assumed that the passive scalar has a Gaussian pdf. Indeed, the pdf of the passive scalar field from the present DNS is very close to Gaussian, as is attested by the skewness and flatness factors ($S_\theta = 0.015$ and $F_\theta = 3.15$). This agrees with the results from numerous other DNS of isotropic turbulence with passive scalars, e.g. [30, 40]. Moreover, this assumption is consistent with the commonly assumed clipped Guassian pdf shape for the mixture fraction in turbulent reactive flows [35]. It must be stressed, however, that in many situations the pdf of the scalar field is highly non-Gaussian. A well-known example is the passive scalar pdf near the edge of a free shear flow, where the scalar has different values inside and outside the shear layer. For relatively low values of the Reynolds number, the mixing near the shear layer edge is governed by the intermittent nature of this interface and the scalar pdfs exhibit a so-called 'marching behaviour', where the pdf maximum moves as one moves across the shear layer [41].

The blackbody radiation intensity is only a function of temperature, while the absorption coefficient depends on the temperature and on the molar fraction of $CO_2$. Since the mean value

and the variance of these scalars are prescribed and the scalars are fully correlated, the time-averaged radiation intensity is computed as follows:

$$\bar{I} = \sum_k \sum_i \omega_i \, \overline{k_{i,k} I_{\mathrm{b},\Delta\nu_k}} \Big/ \bar{k}_{i,k} = \sum_k \sum_i \omega_i \frac{\int_{T_{\min}}^{T_{\max}} k_{i,k}\left(x_{\mathrm{CO}_2}, T\right) I_{\mathrm{b},\Delta\nu_k}(T) p(T) \mathrm{d}T}{\int_{T_{\min}}^{T_{\max}} k_{i,k}\left(x_{\mathrm{CO}_2}, T\right) p(T) \mathrm{d}T}, \tag{24}$$

where

$$x_{\mathrm{CO}_2} = \bar{x}_{\mathrm{CO}_2} + \left(T - \bar{T}\right) \sqrt{\overline{x'^2_{\mathrm{CO}_2}} \Big/ \overline{T'^2}}, \tag{25}$$

and $p(T)$ is the pdf of the temperature, whose shape is assumed to be Gaussian, as stated above.

The mean blackbody radiation intensity and the Planck-mean absorption coefficient may be estimated as follows:

$$\bar{I}_{\mathrm{b}} = \frac{\sigma \overline{T^4}}{\pi} = \frac{\sigma}{\pi} \int_{T_{\min}}^{T_{\max}} T^4 p(T) \mathrm{d}T, \tag{26}$$

$$\overline{\kappa_P^n} = \int_{T_{\min}}^{T_{\max}} \left( \frac{\int_0^\infty \kappa_\nu \, I_{\mathrm{b}\nu} \, \mathrm{d}\nu}{\int_0^\infty I_{\mathrm{b}\nu} \, \mathrm{d}\nu} \right)^n p(T) \, \mathrm{d}T = \int_{T_{\min}}^{T_{\max}} \left( \frac{\sum_k \sum_i \omega_i k_{i,k} \, I_{\mathrm{b},\Delta\nu_k}}{\sum_k I_{\mathrm{b},\Delta\nu_k}} \right)^n p(T) \, \mathrm{d}T, \tag{27}$$

with $n = 1$. Higher order moments of the Planck-mean absorption coefficient, namely the rms, $(\overline{\kappa_{\mathrm{P}}'^2})^{1/2}$, the skewness, $\overline{\kappa_{\mathrm{P}}'^3}/(\overline{\kappa_{\mathrm{P}}'^2})^{3/2}$ and the flatness, $\overline{\kappa_{\mathrm{P}}'^4}/(\overline{\kappa_{\mathrm{P}}'^2})^2$, may be estimated using equation (27) and noting that

$$\overline{\kappa_{\mathrm{P}}'^2} = \overline{\kappa_{\mathrm{P}}^2} - \bar{\kappa}_{\mathrm{P}}^2, \tag{28a}$$

$$\overline{\kappa_{\mathrm{P}}'^3} = \overline{\kappa_{\mathrm{P}}^3} - 3\overline{\kappa_{\mathrm{P}}^2}\bar{\kappa}_{\mathrm{P}} + 2\bar{\kappa}_{\mathrm{P}}^3, \tag{28b}$$

$$\overline{\kappa_{\mathrm{P}}'^4} = \overline{\kappa_{\mathrm{P}}^4} - 4\overline{\kappa_{\mathrm{P}}^3}\bar{\kappa}_{\mathrm{P}} + 6\overline{\kappa_{\mathrm{P}}^2}\bar{\kappa}_{\mathrm{P}}^2 - 3\bar{\kappa}_{\mathrm{P}}^4. \tag{28c}$$

The emission term of the time-averaged form of the RTE is estimated as

$$\overline{\kappa_{\mathrm{P}} I_{\mathrm{b}}} = \sum_k \sum_i \omega_i \, \overline{k_{i,k} \, I_{\mathrm{b},\Delta\nu_k}} = \sum_k \sum_i \omega_i \int_{T_{\min}}^{T_{\max}} k_{i,k}(x_{\mathrm{CO}_2}, T) I_{\mathrm{b},\Delta\nu_k}(T) p(T) \, \mathrm{d}T. \tag{29}$$

## 3. Results and discussion

In this section, we analyse the variables governing the radiative heat transfer such as its topology, one point statistics and spectra. To the author's knowledge, this paper presents the first detailed characterization of these quantities in isotropic turbulence. It is well known that in studies of turbulence physics, the detailed characterization of the governing flow features such as the vorticity, pressure or viscous dissipation rate has allowed the development of important tools, which led directly to the development of turbulence models for the subgrid scales of motion or

the evolution of spectral closures. One of the objectives of the present work is to present and analyse similar features for the radiative transfer quantities with the goal to analyse potential new directions for modelling TRI.

In the second part of this section, we assess the influence of several parameters such as the optical thickness of the medium, mean temperature of the medium or the variance of the temperature in the statistics of the TRI governing variables. Before this, it is important to describe the physical parameters of the reference calculations.

### *3.1. Description of the standard properties of the medium*

Radiative transfer calculations were carried out assuming that the mean temperature of the medium is 1500 K, and that the medium is a mixture of $CO_2$ and radiatively transparent species, the mean molar fraction of $CO_2$ being 0.10. The rms of temperature and of $CO_2$ molar fraction were taken as 150 K and 0.01, respectively, and the optical thickness of the medium is equal to $\tau = 1$. These values were chosen to represent physical conditions, which are typical of the far-field self-preserving region of a turbulent reacting jet, downstream of the location where combustion has taken place. We label this case as the *standard radiative transfer calculation* (SRTC), and we will use it as a reference for comparisons throughout this paper. The values of rms are relatively small, and larger values are often found in combustion applications. However, if higher values are chosen, local instantaneous temperatures or molar fractions obtained from rescaling DNS data by means of equations (8) and (9), respectively, may be unrealistic, since scalar fluctuations in DNS are unbounded. For example, the temperature may exceed typical adiabatic flame temperatures of hydrocarbons burning in air at atmospheric conditions or local instantaneous molar fractions may decrease below zero. Although such unphysical values could be prevented by prescribing limits to the range of allowable temperatures and molar fractions, this would modify the statistical data generated from DNS. Therefore, to prevent unrealistic local instantaneous temperatures or molar fractions to appear, and to preserve the statistical data from DNS, the relatively low rms values given above were considered in the present paper.

Figure 2 shows the normalized values of the mean (non-dimensionalized by the blackbody radiation intensity), rms (non-dimensionalized by the mean radiation intensity), skewness and flatness of the radiation intensity leaving the computational domain as a function of the number of instantaneous fields

$$\bar{I}\big/I_b(\bar{T}), \quad (\overline{I'^2})^{1/2}\big/\bar{I}, \quad \overline{I'^3}\big/(\overline{I'^2})^{3/2}, \quad \overline{I'^4}\big/(\overline{I'^2})^2. \tag{30}$$

The results plotted in figure 2 show that $N_t = 1$ is sufficient to accurately determine the normalized mean and rms of the radiation intensity, but is not enough to obtain statistically independent results for the skewness and flatness. However, when $N_t$ exceeds 20–25 the influence of $N_t$ on the results becomes marginal. The pdfs of the radiation intensity and of the Planck-mean absorption coefficient, which are given in figure 3 for $N_t = 10$, 20, 30 and 40, confirm the good convergence of the results for $N_t = 40$. Therefore, we conclude that the statistics for these variables are well converged when $N_t = 40$ and all the subsequent analysis was carried out using $N_t = 40$ instantaneous fields.

### *3.2. Characterization of the radiative transfer variables in isotropic turbulence*

We start the characterization of the radiative heat transfer variables in isotropic turbulence by using instantaneous contour plots taken at one of the boundaries of the computational domain.

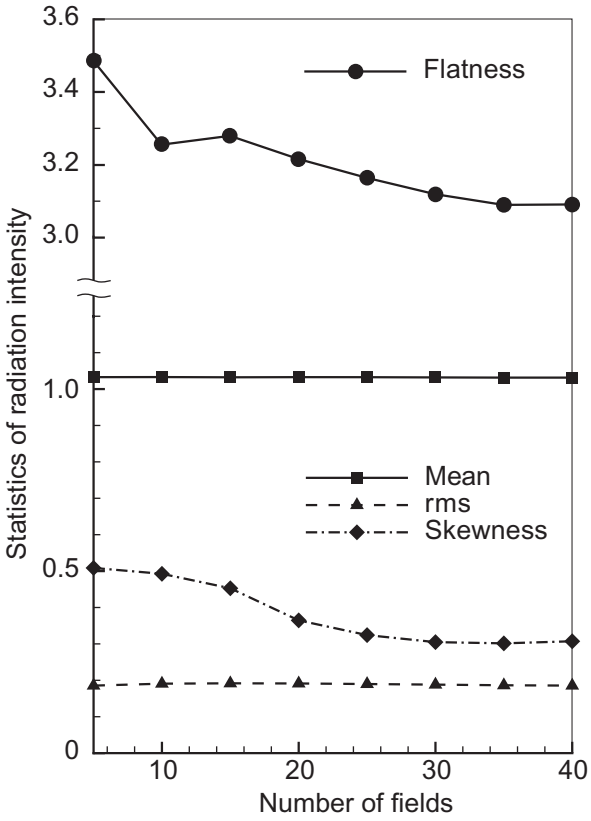


**Figure 2.** Radiation intensity as a function of the number of instantaneous fields.

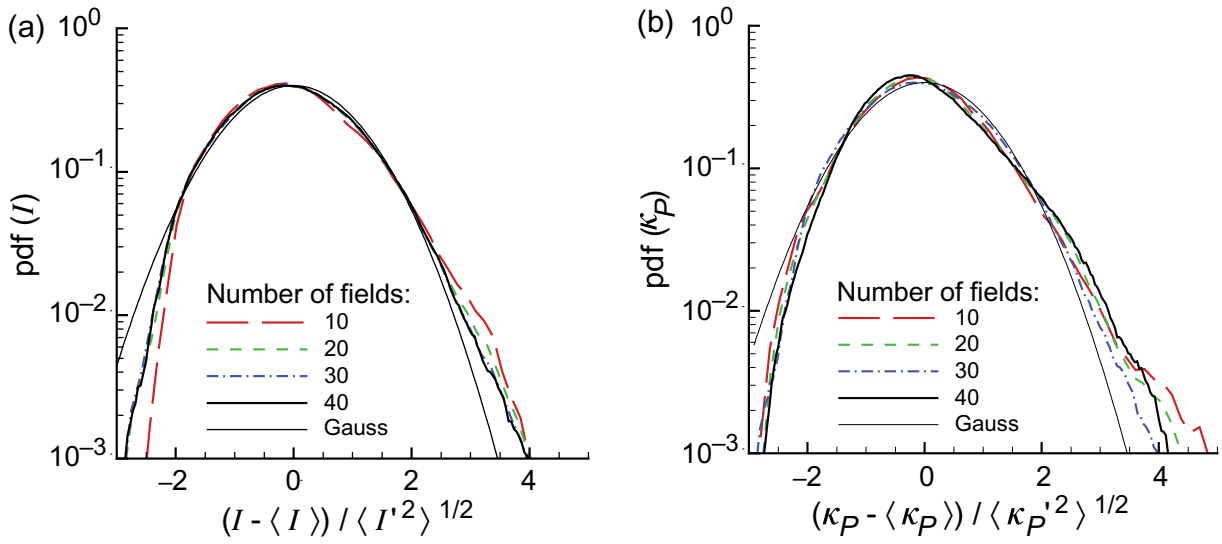


**Figure 3.** Pdfs of the radiation intensity and Planck-mean absorption coefficient as a function of the number of instantaneous fields, $N_t$.

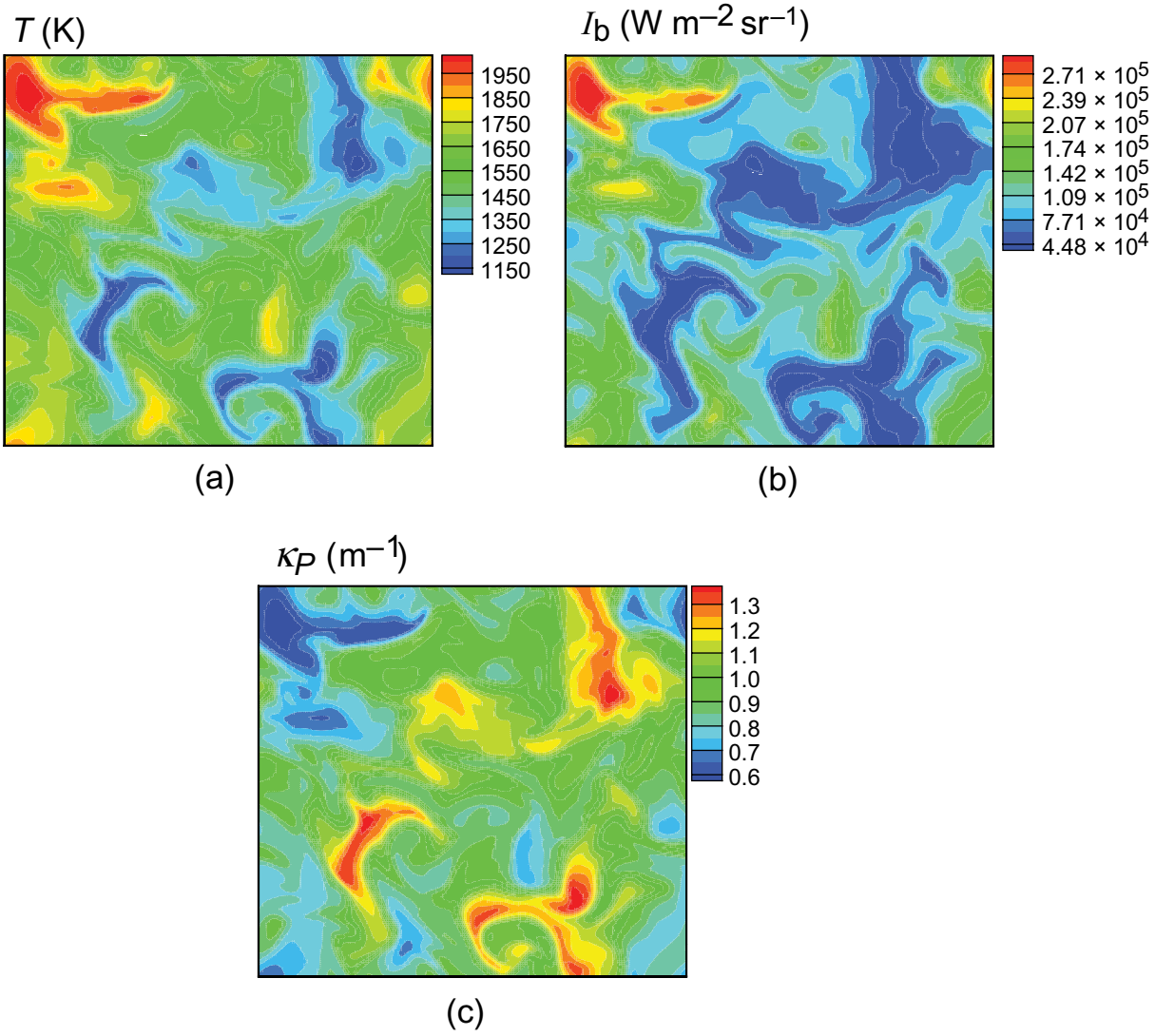


**Figure 4.** Instantaneous contour plots of temperature, blackbody radiation intensity and Planck-mean absorption coefficient at one of the boundaries of the computational domain.

Figure 4 shows instantaneous contour plots of temperature, blackbody radiation intensity and Planck-mean absorption coefficient.

The temperature field shows the existence of sharp gradients across lengths of the order of the integral scale $L_{11}$, and displays the well-known 'ramp-cliff' structures typical of the passive scalar fields in turbulent flows and that are generated by the tearing effect of the large scale vortices [22]. Not surprisingly the blackbody radiation intensity displays a similar structure since the blackbody radiation intensity is proportional to the fourth power of temperature, and therefore these two variables are strongly correlated, as suggested by their contour plots. The Planck-mean absorption coefficient depends on $T$ and on the molar fraction of $CO_2$. In the present work, the molar fraction of $CO_2$, like the temperature field, is obtained directly from the passive scalar field generated from the DNS data. It follows that both $T$ and the molar fraction

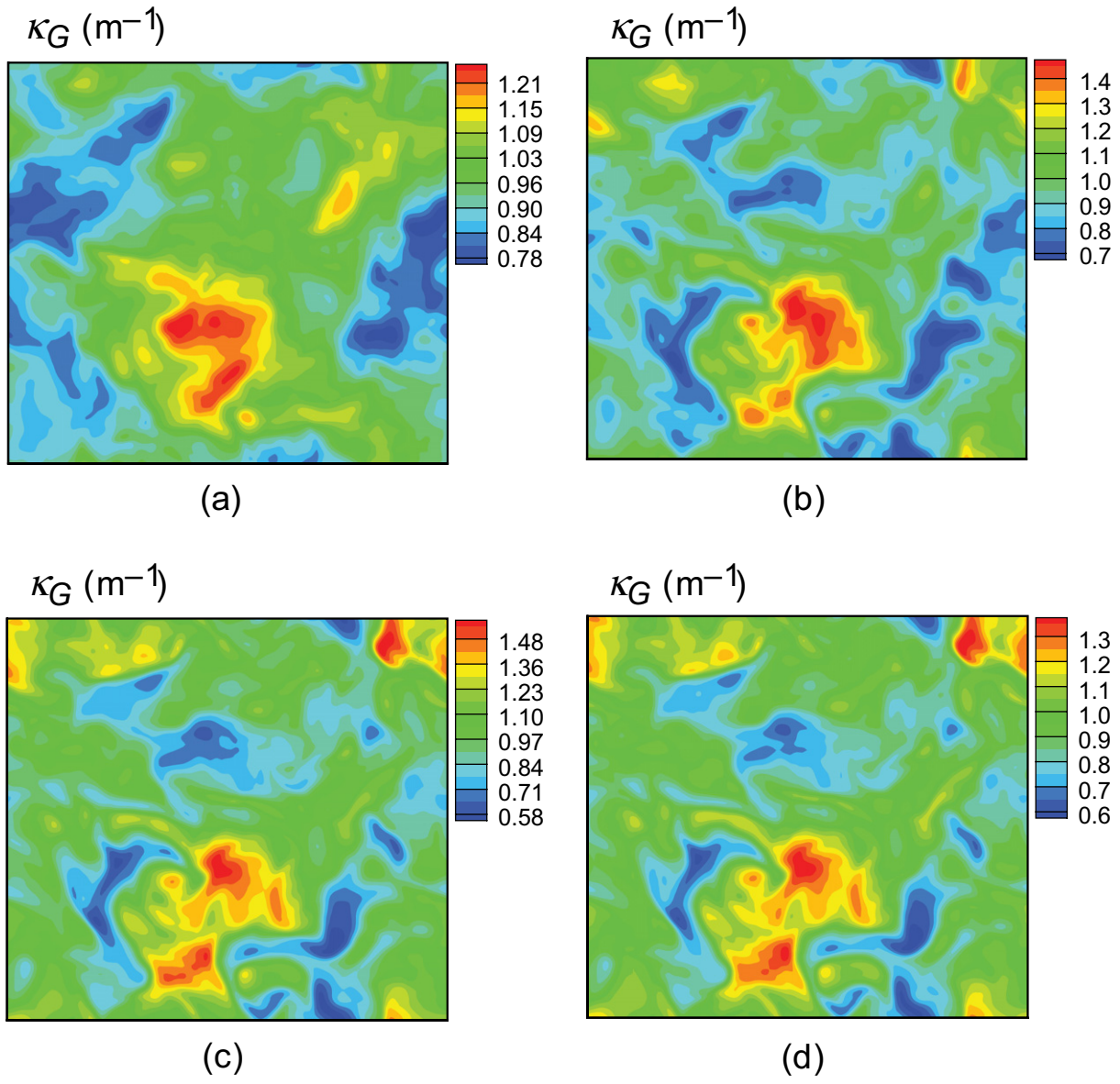


**Figure 5.** Instantaneous contour plots of incident-mean absorption coefficient ($\kappa_G$) at one of the boundaries of the computational domain for four values of the optical thickness of the medium: (a) $\tau = 0.1$, (b) $\tau = 1.0$, (c) $\tau$=10 and (d) $\tau = 100$.

of $CO_2$ are strongly correlated, which leads to the strong correlation between $\kappa_P$ and $T$ that can be seen in the figures. However, since $\kappa_P$ decreases with the increase of $T$ (for the range of temperature and for the species under consideration), we observe a strong negative correlation between these quantities, i.e. $T$ (or $I_b$) and $\kappa_P$ are anti-correlated. The contour plots support this conclusion.

The contour plots of the incident-mean absorption coefficient are shown in figure 5 for several values of the optical thickness of the medium $\tau$. For small values of $\tau$ ($\tau = 0.1$ or 1.0), $\kappa_G$ shows no apparent relation with any of the other flow variables (see figures 5(a) and (b)).

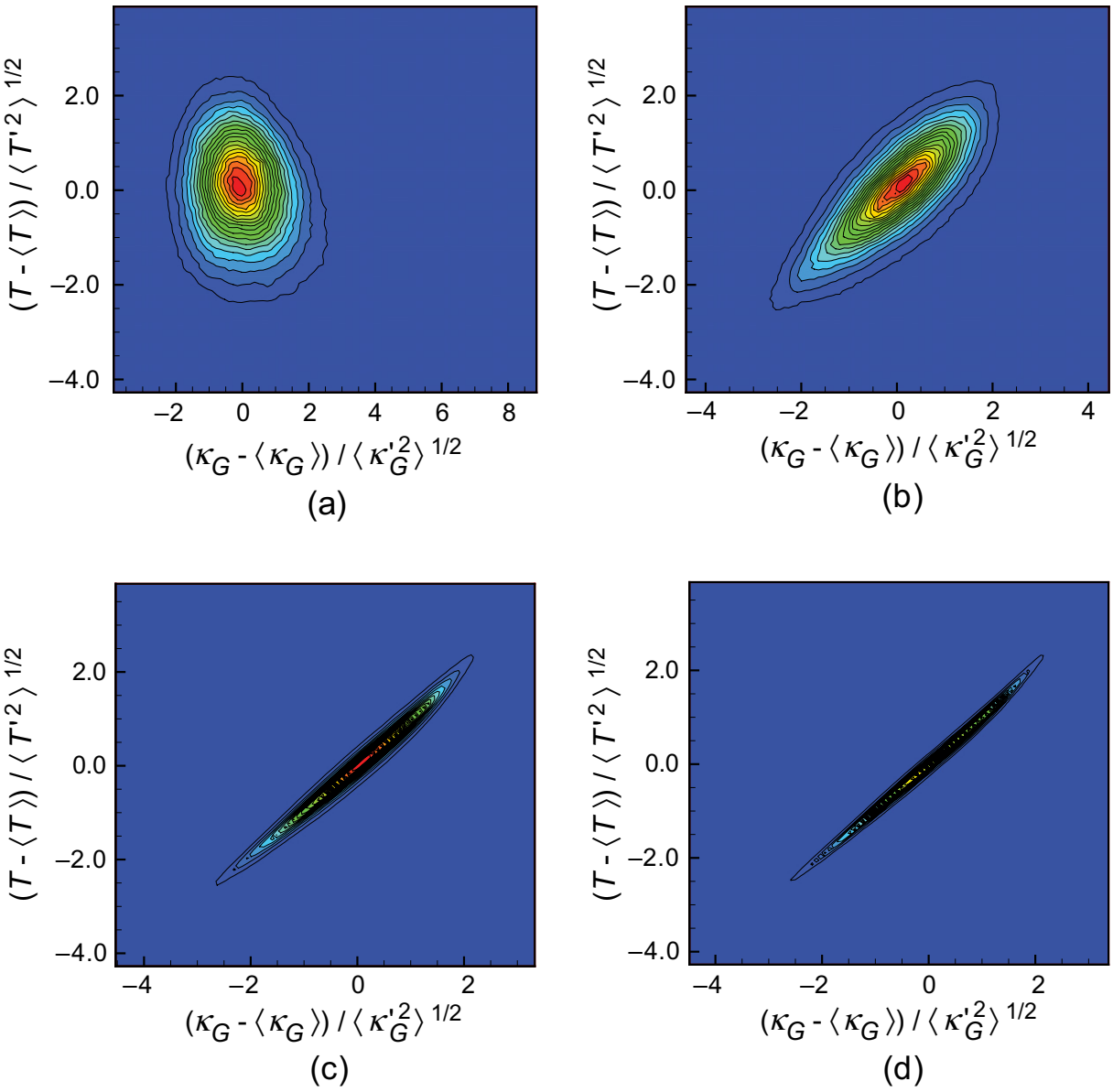


**Figure 6.** Joint pdf of the incident-mean absorption coefficient and temperature as a function of the optical thickness of the medium: (a) $\tau = 0.1$, (b) $\tau = 1.0$, (c) $\tau = 10$ and (d) $\tau = 100$.

This can be explained by the fact that $\kappa_G$ depends on the local temperature and molar fraction of $CO_2$, but also on the properties along the optical path, due to its dependence on $I_\nu$ (see equation (13)). However, for large values of the optical thickness of the medium ($\tau = 10$ or 100), the effect of the local temperature dominates and $\kappa_G$ displays a topology similar to the temperature field (compare figures 4(a) and 5(d)). This fact can be attested by the correlation coefficients between these quantities, which take the values of 0.75, 0.98 and 0.99 for $\tau = 1.0$, 10 and 100, respectively. The corresponding joint pdfs are shown in figure 6 and support this conclusion.

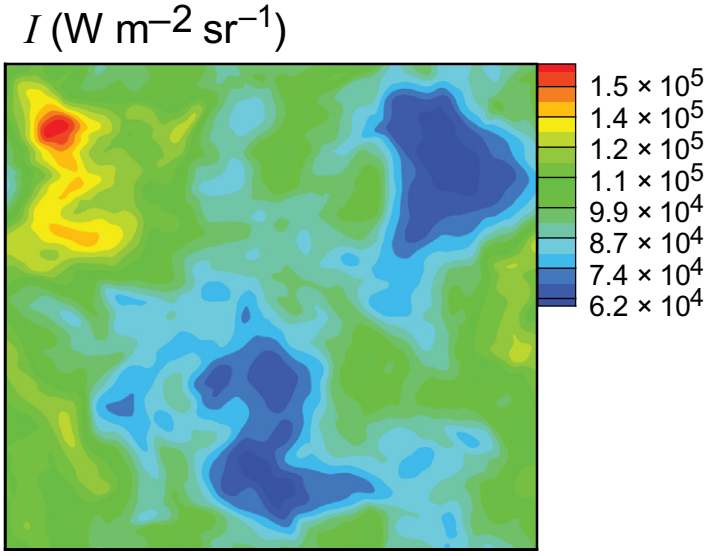


**Figure 7.** Instantaneous contour plot of radiation intensity at one of the boundaries of the computational domain.

Figure 7 shows an instantaneous contour plot of radiation intensity for the SRTC, at one of the boundaries of the computational domain. This quantity displays no significant correlation with any one of the other variables. In fact, in contrast to $I_b$, the radiation intensity at a grid node depends on the temperature and $CO_2$ molar fraction at all upstream grid nodes along the optical path, and not only on local properties. The structures of $I$ exhibit coherence over a large fraction of the flow domain, i.e. over a distance significantly larger than the integral scale for the velocity and scalar fields, which here is about one-fifth of the box size. This suggests that a relatively coarse mesh might be sufficient to give a sufficiently good description of this variable in numerical simulations of TRI, i.e. a grid coarser than the corresponding grid needed to carry out an accurate DNS or LES of the associated turbulent velocity and scalar fields.

### *3.3. The spectra of thermal radiation variables*

The existence of power laws has proved extremely important in the context of the turbulence theory and it is plausible that the application of the classical tools from isotropic turbulence theory in this context might help to obtain universal laws of the radiation intensity that are useful for future TRI modelling studies, e.g. Soufiani [24] analysed the effects of radiation on the evolution of the temperature field in isotropic turbulence.

If a power law $I \sim k^{-\alpha}$ were to exist, this would allow the development of subgrid-scale models for the RTE. Kounalakis *et al* [3, 42] measured temporal (1D) power spectra from the radiation intensity in a turbulent reacting jet at $x/D = 50$, 90 and 130. Their results showed that the slope $\alpha$ of the power spectra of the radiation intensity decreases slowly with the downstream distance, and for $x/D = 130$ they found a power law close to $-5/2$, i.e. somewhat steeper than the classical $-5/3$ law from the turbulence related quantities. No satisfactory explanation was given for this behaviour. It was argued that the radiation intensity is affected by the broad range of space and timescales that exists along the optical path, but is dominated by the highest temperatures along that path. Since the temperature field exhibits a $-5/3$ inertial range, they argued that the radiation intensity should obey a similar law.

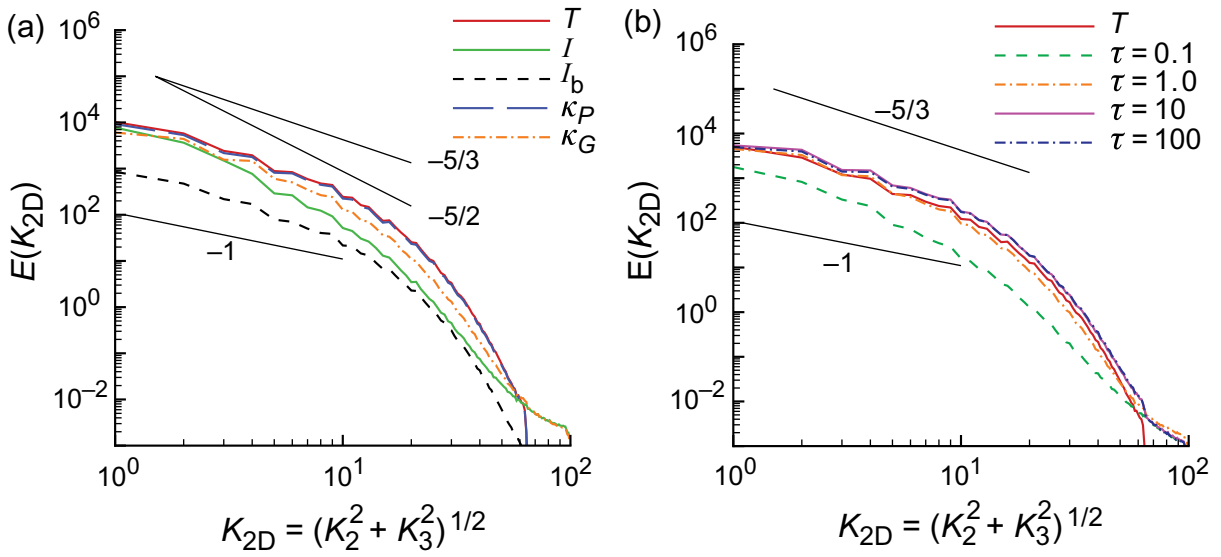


**Figure 8.** Spectra computed using a 2D plane taken from a single instantaneous field. Lines with slopes of $-5/3$, $-5/2$ and $-1$ are also shown for comparison. (a) Spectra of temperature, blackbody radiation intensity, radiation intensity, Planck-mean absorption coefficient and incident-mean absorption coefficient. (b) Spectra of the incident-mean absorption coefficient as a function of the optical thickness of the medium, $\tau$. The temperature spectrum is plotted again for comparison.

One-dimensional frequency spectra of the radiation intensity downstream of a turbulent jet flame were also reported by Zheng *et al* [43] and by Zheng and Gore [44]. Their results reveal the existence of a power-law region, but unfortunately the spectral slopes were not measured or discussed. However, one can see from their data that different flames show different spectral slopes for the same axial position, which implies that the spectrum of $I$ does not depend only on the kinematic and temperature characteristics of the jet. Using a turbulent jet flame at a larger Reynolds number than in the references above, Kounalakis *et al* [13] observed a large $-5/3$ inertial range region spanning about two decades in the spectra of the radiation intensity. No explanation was given, however.

As illustrated by the works referenced above, no systematic study of this problem exists at present. In the present work, we used a DNS data bank to compute 2D spatial spectra of the radiation intensity and other quantities governing radiative heat transfer, such as the temperature, blackbody radiation intensity, Planck-mean and incident-mean absorption coefficients. The spectra are displayed in figure 8(a). In order to facilitate comparisons, all the spectra were non-dimensionalized to show similar values for the wavenumber $k = 1$. These spectra were computed using 2D planes averaged over 40 fields.

All the spectra exhibit an energy-containing region, an intermediate region, and a final region where the energy decreases with a nearly exponential decay. Note that it is this fact, i.e. the higher radiative energy is associated with small wavenumbers (large scales), that makes possible the development of 'large-eddy simulations' of the radiative heat transfer [18].

As expected from the above discussion the spectral shapes of the temperature, blackbody radiation intensity, and Planck-mean absorption coefficient are very similar and display the

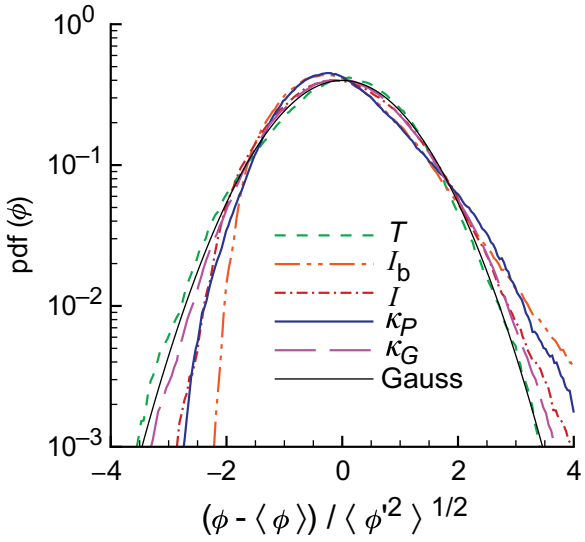


**Figure 9.** Pdfs of temperature, blackbody radiation intensity, radiation intensity, Planck-mean absorption coefficient and incident-mean absorption coefficient. A Gaussian pdf is also shown for comparison. All the pdfs were obtained using $N_t = 40$ instantaneous fields.

characteristic (although short) inertial range with a $-5/3$ power law. For intermediate and high wavenumbers the incident-mean absorption coefficient has significantly less energy. It seems that the effect of the non-local contribution is to smooth out the energy from the intermediate and high frequencies from $\kappa_G$. This 'pseudo-dissipation' effect caused by the contribution of non-local physics is even more intense in the radiation intensity. Indeed, one clearly sees in figure 8(a) that the spectral distribution of $I$ displays comparatively less energy than the other variables over the entire wavenumber range, again showing the less stringent resolution requirements for the radiation intensity as compared with other flows variables, such as the temperature field, which exhibits stronger spatial gradients.

The present results show a power-law region for the radiation intensity. The figure suggests that the spectral slope is closer to $-5/2$ than to the classical $-5/3$ observed for turbulence-related quantities. A similar result was observed also by Kounalakis *et al* [3]. We verified that this result is relatively insensitive to the optical thickness, since radiation intensity spectra obtained with several values of the optical thickness did not show an appreciable change in this spectral slope (not shown). On the other hand, $\kappa_G$ did show a marked sensitivity to the optical thickness, as shown in figure 8(b). The spectra of $\kappa_G$ tend to a power law near $-5/3$ as the optical thickness increases, i.e. it seems that a classical power law of $-5/3$ is recovered as the non-local effects decrease (the spectrum of the temperature field is also shown for reference). It is possible that under different conditions, e.g. under smaller non-local effects, the spectrum of the radiation intensity might be close to $-5/3$. Recall that Kounalakis *et al* [13] observed a $-5/3$ power law for the spectrum of the radiation intensity for a high Reynolds number turbulent jet flame. At present no explanation for this behaviour exists. Due to its importance, this issue should be pursued in future works.

To conclude the characterization of the statistical properties of the variables governing the radiative heat transfer, figure 9 displays the pdfs of temperature, blackbody radiation intensity,

radiation intensity, Planck-mean absorption coefficient and incident-mean absorption coefficient for the SRTC. A Gaussian pdf is also shown for comparison. All the pdfs were obtained using $N_t = 40$ instantaneous fields.

It is well known that the pdf of a passive scalar field, such as the temperature, is very nearly Gaussian in isotropic turbulence [30, 45]. More precisely, the temperature (like the velocity field) is slightly subGaussian, and the higher the order of spatial derivatives applied to these quantities the further distant they are from the Gaussian pdf [30, 45]. The nonGaussian nature of the velocity and temperature fields is a well-known fact from turbulence studies and is connected with the presence of a temperature variance (and kinetic energy) cascade from the large down to the small scales of motion. It is interesting to analyse the shape of the pdfs of the variables governing the radiative heat transfer as this will give guidelines for the development of subgrid-scale models for TRI. Figure 9 shows indeed that the temperature is very nearly Gaussian, and the same is true of the Planck-mean absorption coefficient, as expected, since it depends only on the passive scalar field from the DNS used to define both the temperature and the $CO_2$ molar fraction. The blackbody radiation intensity, on the other hand, deviates significantly from the Gaussian shape although being also completely defined by the passive scalar field from the DNS. The shape of this pdf shows that the probability of finding values of $I_b$ greater than the mean value is significantly more important than the probability of finding values of $I_b$ smaller than the mean value, and this explains why the skewness factor of $I_b$ is greater than zero. The explanation lies in its definition through equation (26) where the fourth power of the temperature field increases significantly the importance of the most intense local values of temperature. The pdfs of incident-mean absorption coefficient and radiation intensity have local and non-local effects in their definition, as described above, which tend to smooth the local spatial gradients and act as an additional spatial filter or 'pseudo-dissipation'. This may explain why these quantities still exhibit a non-Gaussian shape with a positive skewness, although with a smaller value than that of the blackbody radiation intensity. Note that, in agreement with the results above, we observed that the pdf of $\kappa_G$ approaches a Gaussian shape as the non-local effects decrease.

### *3.4. Assessment of the influence of the properties of the medium on the TRI*

*3.4.1. Influence of the optical thickness of the medium.* Figure 10(a) shows statistical data for the radiation intensity, normalized as in figure 2, as a function of the optical thickness of the medium. These results were computed from the DNS data, as described in section 2.2, taking $N_t = 40$. Figure 10(a) also shows the normalized time-averaged radiation intensity predicted from equation (24).

The change of the optical thickness of the medium was accomplished by modifying the size of the radiation domain, while keeping $\kappa_P(\bar{T}, \bar{x}_{CO_2})$ unchanged. Another option, which has also been tested, is to fix the size of the domain and to modify $\bar{x}_{CO_2}$. However, while the first option allows the analysis of a wide range of optical thicknesses, which spans over three orders of magnitude, the second one requires a much narrower range. In fact, unphysical negative or greater than unity values of $x_{CO_2}$ may appear when equation (9) is applied if $\bar{x}_{CO_2}$ is close to zero or close to one, respectively. The limited range of $x_{CO_2}$ implies a limited range of optical thicknesses. Moreover, the results obtained exhibit similar trends no matter whether the optical thickness changes due to the variation of the size of the domain or due to the variation of $\bar{x}_{CO_2}$. Accordingly, only the results obtained in the first case are reported below. Note that the flow

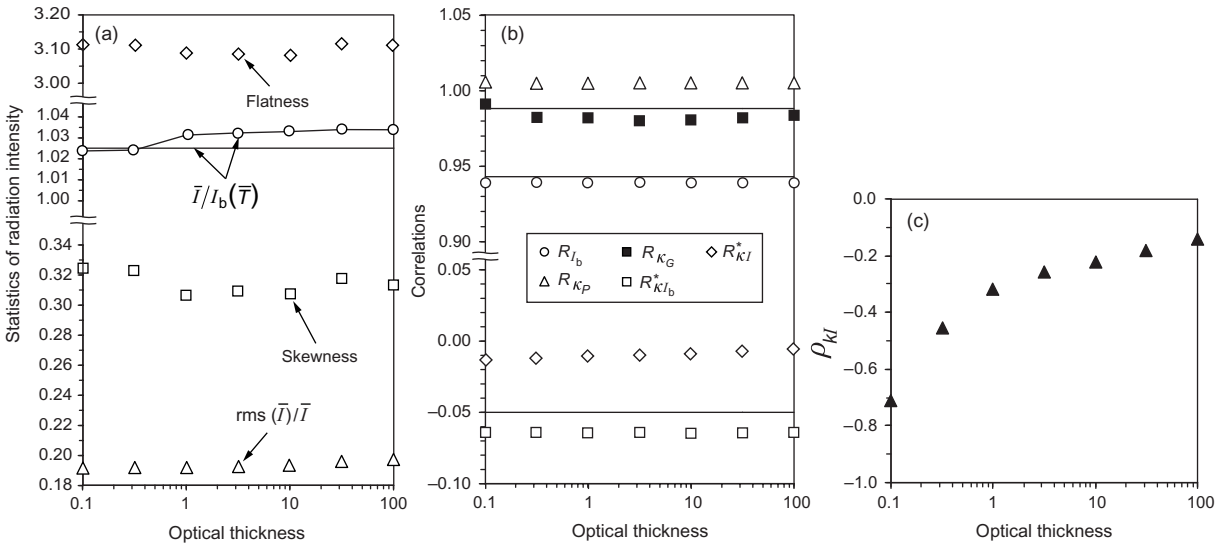


**Figure 10.** Statistics of the radiation intensity as a function of the optical thickness of the medium.

domain for the DNS calculations, as well as the effective length scale of the turbulence, remain unchanged.

Since $\bar{x}_{CO_2}$ is fixed while varying the size of the domain, the mean radiation intensity does not change with the optical thickness, as concluded from equation (24) and shown in figure 10(a). The statistical data exhibit a small change of $\bar{I}$, which may be attributed to statistical errors, but the predictions based on the solution of equation (24) do not. The rms of the radiation intensity increases marginally when the optical thickness of the medium changes from 0.1 to 100. The skewness is different from zero, i.e. the pdf is slightly asymmetric and shifted to the right, as formerly observed in figure 3. The flatness is just a little above 3, which means that at least concerning the levels of intermittency the pdf is very close to Gaussian. These moments of the radiation intensity also remain approximately constant when the optical thickness varies, while keeping $\kappa_P(\bar{T}, \bar{x}_{CO_2})$ unchanged.

Figure 10(b) shows the influence of the optical thickness on several correlations defined in equation (19). The predictions of $R_{I_b}$, $R_{\kappa_P}$ and $R^*_{kI_b}$, which were obtained making use of equations (26)–(29), are also shown. The marginal variation of the reported quantities with the optical thickness is expected, since neither $\bar{T}$ nor $\bar{x}_{CO_2}$ has been changed. It can be seen that $R_{I_b} < 1$, i.e. turbulent fluctuations cause an increase of the mean blackbody radiation intensity in comparison with laminar flows, as is widely known [2]. In the present case, the increase is only about 6%, because the prescribed rms of temperature is just 10% of the mean temperature. However, it has been shown that temperature fluctuations of ±20% increase the mean blackbody radiation intensity by 24%, while temperature fluctuations of ±30% yield an increase of more than 50% [46]. Fluctuations of this order of magnitude may be found in combustion systems. The prediction of $R_{I_b}$ based on an assumed Gaussian scalar pdf is rather satisfactory. The prediction of $R_{k_P}$ is not as accurate as observed for $R_{I_b}$. In fact, even though the error in the prediction of $R_{k_P}$ is lower than 2%, the predictions yield $R_{k_P} < 1$, in contrast to the statistical data, which give $R_{k_P} > 1$. Despite of this, the influence of TRI in $\bar{\kappa}_P$ is rather small for the studied conditions, as concluded from both the statistical data and the predictions.

It was mentioned above that $\kappa_P$ and $I_b$, which are local quantities, are anti-correlated. Therefore, $\overline{\kappa' I'_b} < 0$, yielding $R^*_{kI_b} < 0$, in agreement with figure 10(b). The predictions obtained from equations (26)–(29) reproduce this behaviour. In contrast to $I_b$, the radiation intensity is not a local quantity, but depends on the temperature and species concentrations along the optical path. As a consequence of this, the correlation between the incident-mean absorption coefficient and the radiation intensity is expected to be small. The results show that $R_{kI_b}$ is indeed small, ranging between $-0.013$ for an optical thickness of 0.1 and $-0.006$ for an optical thickness of 100, which justifies the OTFA.

Further insight into this issue is provided by the correlation coefficient between the incident-mean absorption coefficient and the radiation intensity, $\rho_{kI}$, shown in figure 10(c). The joint pdf between these two variables for selected values of the optical thickness of the medium is shown in figure 11. Both figures reveal a clear trend towards an increase, in absolute value, of $\rho_{kI}$ when the optical thickness of the medium decreases. This trend may seem surprising, since it would be expected that the correlation coefficient approached zero in the limit of an optically thin medium. This is the reasoning underlying the OTFA, which is supported, e.g. by DNS results reported in [25]. Moreover, the correlation coefficient, in absolute value, is actually higher than one might expect, since the radiation intensity is not a local quantity.

The explanation for the behaviour reported above is probably related to the nature of the problem under investigation. In fact, since the medium is homogeneous and isothermal, if there were no turbulent fluctuations, equation (16) could be written as

$$I_{i,\Delta\nu_k}(s) = I_{i,\Delta\nu_k}(0)\exp(-k_{i,k}\,s) + [1 - \exp(-k_{i,k}\,s)]I_{b,\Delta\nu_k}. \tag{31}$$

This yields $I_{i,\Delta\nu_k}(s) = I_{b,\Delta\nu_k}$ if the periodic boundary condition is enforced. Therefore, the radiation intensity tends to the blackbody radiation intensity if there are no turbulent fluctuations. Moreover, the blackbody radiation intensity and the Planck-mean absorption coefficient are strongly correlated, since they depend only on local properties. Although $I_{i,\Delta\nu_k}(s)$ is actually different from $I_{b,\Delta\nu_k}$ due to turbulence, it is not substantially different, because the medium is statistically homogeneous and isothermal, and so $\rho_{kI}$ is likely to be higher than in non-homogeneous and/or non-isothermal media. In addition, it can be shown that if $s \to 0$ and $I_{i,\Delta\nu_k}(0)$ is set equal to $I_{i,\Delta\nu_k}(s)$, then $I_{i,\Delta\nu_k}(s)$ given by equation (16) tends to $I_{b,\Delta\nu_k}(s)$. Hence, in the limit of an optically thin medium with periodic boundary conditions, $\rho_{kI}$ is expected to be high, which explains the observed increase in absolute value of $\rho_{kI}$ when the optical thickness of the medium decreases.

*3.4.2. Influence of the temperature of the medium.* Figure 12 shows the influence of the mean temperature of the medium on the radiation statistics and relevant TRI correlations. The rms of temperature was also changed to keep $\overline{T'^2}/\bar{T}^2$ constant. The optical thickness of the medium is maintained equal to unity. Since the Planck-mean absorption coefficient depends on the temperature, it will change, and therefore the size of the domain changes as well to keep the optical thickness constant.

The mean radiation intensity decreases if the temperature increases, in agreement with the results in [14], and this trend is correctly predicted from equation (24) with the assumption of a Gaussian scalar pdf. The main contribution to $\bar{I}$ comes from the 4.3 $\mu$m band of $CO_2$. If the temperature increases, the fraction of blackbody radiative energy emitted in this band is lower, as a result of Wien's law. This justifies the observed evolution of $\bar{I}(T)$. The influence of the temperature on the rms of the radiation intensity is marginal. In addition, figure 12(a) shows

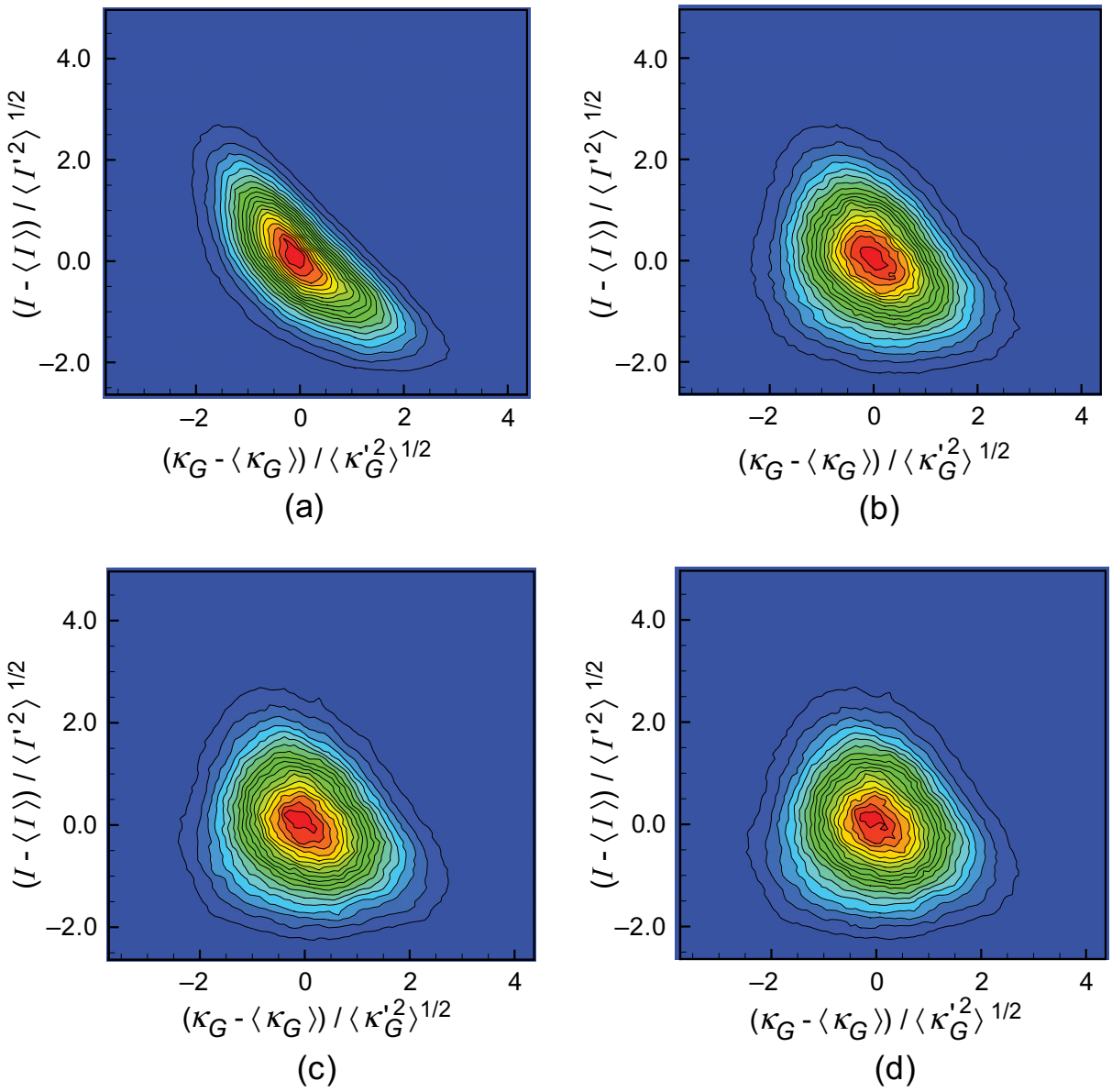


**Figure 11.** Joint pdf of the incident-mean absorption coefficient and radiation intensity as a function of the optical thickness of the medium: (a) $\tau = 0.1$, (b) $\tau = 1.0$, (c) $\tau = 10$ and (d) $\tau = 100$.

that the skewness and the flatness are close to those found for standard conditions, except at $\bar{T} = 1650\,\mathrm{K}$, where both the skewness and the flatness indicate that the pdf of the radiation intensity is not as close to a Gaussian as in the other cases.

Figure 12(b) shows that $\bar{\kappa}_\mathrm{P}$ decreases with the increase of the temperature, as pointed out above. Still, the rms of $\kappa_\mathrm{P}$ does not change significantly. The skewness and the flatness are close to 0 and 3, respectively, for temperatures greater than or equal to 1200 K. However, they significantly depart from those values, which hold for a Gaussian pdf, at $\bar{T} = 900\,\mathrm{K}$. Nevertheless, the prediction of the moments of $\kappa_\mathrm{P}$ remains quite satisfactory if the pdf of temperature is taken as Gaussian.

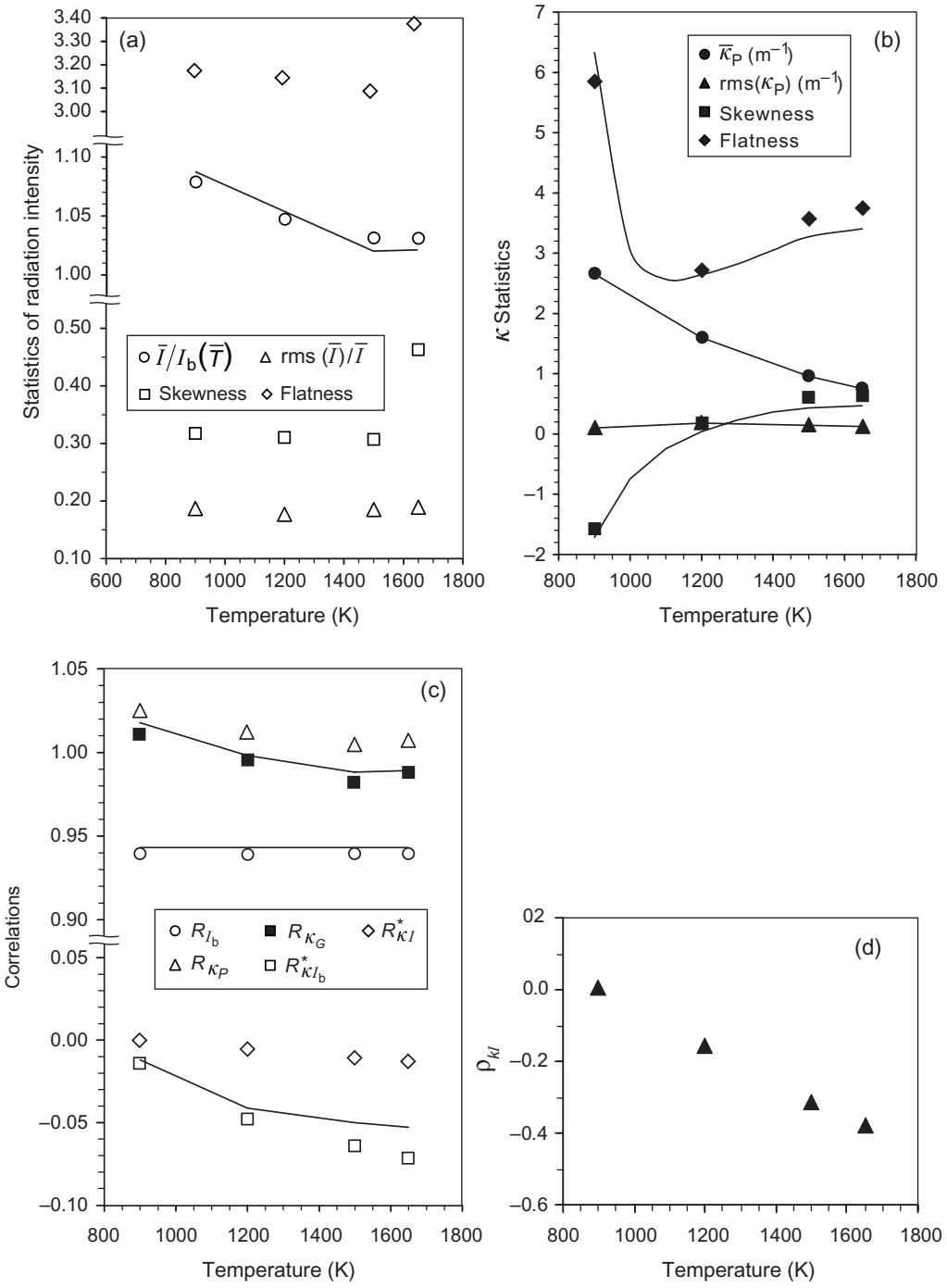


**Figure 12.** Statistics of radiation intensity as a function of the mean and rms of the temperature of the medium (constant ratio of the mean to the rms of the temperature).

Figure 12(c) shows that $R_{I_b}$ is constant, as expected, since $\overline{T'^2}/\bar{T}^2$ does not change, and the predictions closely match the value obtained from DNS. However, the prediction of $R_{\kappa_P}$ is not so good, as also found in section 3.4.1, even though the trend is correctly reproduced.

The variation of $R^*_{kI_b}$ may be explained noting that, making use of equation (23), the following relations hold:

$$R^*_{kI_b} = 1 - \frac{\bar{\kappa}_P \bar{I}_b}{\overline{\kappa_P I_b}} = 1 - \frac{\bar{\kappa}_P}{\bar{\kappa}_G}\frac{\bar{I}_b}{\bar{I}} = 1 - \frac{R_{k_G}}{R_{k_P}}\frac{1}{R_{I_b}}\frac{I_b(\bar{T})}{\bar{I}}. \tag{32}$$

The ratio $R_{\kappa_G}/R_{\kappa_P}$ is approximately independent of the temperature, while $R_{I_b}$ is constant. Moreover, $I_b(\bar{T})/\bar{I}$ increases with the increase of $\bar{T}$, as shown in figure 12(a), and so $R^*_{kI_b}$ decreases when $\bar{T}$ increases, in agreement with the results shown in figure 12(c). The negative values of $R^*_{kI_b}$ are expected, as discussed in section 3.4.1. Figure 12(c) also shows that $R^*_{kI}$ and $R^*_{kI_b}$ behave similarly, although the values of $R^*_{kI}$ are quite low, as expected. The correlation coefficient $\rho_{kI}$ exhibits a similar trend, but with a stronger temperature dependence.

Figure 13(a) shows the influence of the mean temperature of the medium, leaving the rms of temperature unchanged (150 K), on the moments of the radiation intensity. The mean radiation intensity decreases if the temperature increases, as observed also when both the mean and the rms of temperature were changed. This evolution is well predicted using equation (24). In the present case, $\bar{I}/I_b(\bar{T})$ achieves higher values for mean temperatures equal to 900 and 1200 K, because the intensity of turbulent temperature fluctuations, estimated as $\mathrm{rms}(T)/\bar{T}$, is higher and increases with the decrease of the mean temperature. This is also the reason why the normalized rms of the radiation intensity decreases with the increase of the mean temperature. The skewness and flatness are also higher for mean temperatures below 1500 K. The evolutions of $\bar{I}/I_b(\bar{T})$ and $\mathrm{rms}(I)/\bar{I}$ as a function of the mean temperature are in agreement with the results of Kritzstein and Soufiani [14].

The mean and rms of $\kappa_P$, shown in figure 13(b), display the expected trend, which can be explained using the same arguments given above, namely the anti-correlation between $\kappa_P$ and $T$, and the increase of intensity of temperature fluctuations for lower temperatures. The skewness and flatness have a more irregular behaviour, but all the moments are satisfactorily estimated using equations (27) and (28), particularly the lowest ones.

The evolutions of $R_{I_b}$ and $R_{\kappa_P}$ as a function of the temperature, plotted in figure 13(c), reveal that both quantities depart from unity as the intensity of the temperature fluctuations increases. However, while turbulent fluctuations contribute to increase $\bar{I}$, they yield a decrease of $\bar{\kappa}_P$ in comparison with laminar flows. Therefore, $R_{I_b}$ and $R_{\kappa_P}$ exhibit opposite evolutions as the temperature changes. The evolution of $R^*_{kI_b}$, which is not significantly influenced by the temperature, is reasonably well estimated from equations (26)–(29), even though it is not monotonic. This is a consequence of the different behaviour of the various terms in equation (32). Hence, while $\bar{I}_b$ and $\overline{\kappa_P I_b}$ increase with the increase of the temperature, as well as $I_b(\bar{T})/\bar{I}$, $\bar{\kappa}_P$ has as an opposite trend, as well as $R_{\kappa_G}/R_{\kappa_P}$ and $1/R_{I_b}$. The values of $R^*_{kI}$ are about $-0.01$, with a marginal influence of the mean temperature, while $\rho_{kI}$ is negative and increases in absolute value with the increase of the mean temperature. These evolutions are identical to those reported in the previous case, where both $\bar{T}$ and $\mathrm{rms}(T)$ were changing.

*3.4.3. Influence of the variance of the temperature.* The influence of the variance of temperature is shown in figure 14. In this case, $\bar{T} = 1500$ K, and so the intensity of temperature fluctuations is changing. The increase of the temperature fluctuations yields an increase of both the mean and rms of radiation intensity, as expected [2, 14]. The increase is about 3% for the mean radiation intensity if the turbulence intensity is 10%. The predictions based on the

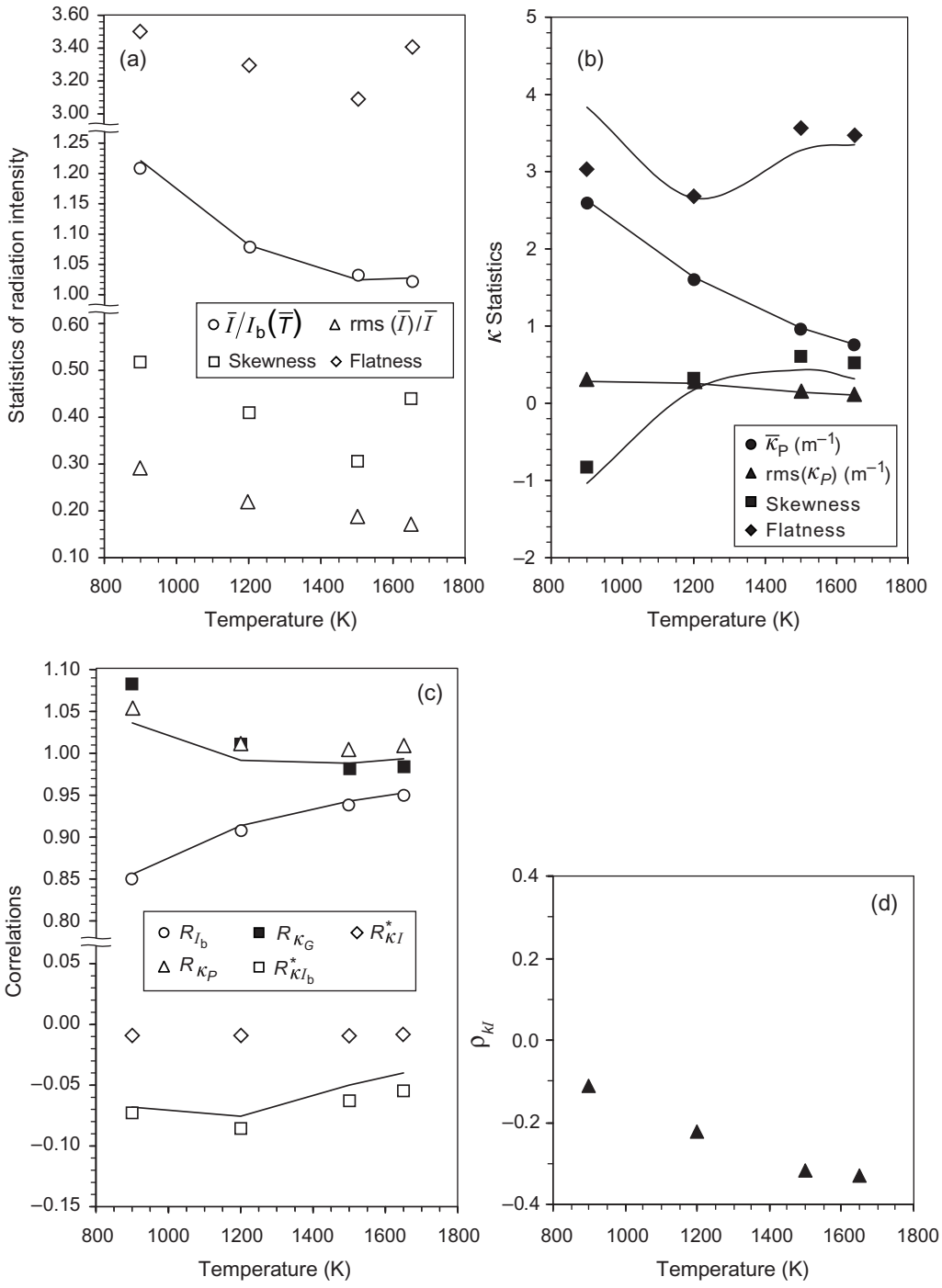


**Figure 13.** Statistics of the radiation intensity as a function of the mean temperature of the medium.

time-averaged RTE reproduce the observed trend. The skewness of the radiation intensity increases with the increase of the rms of temperature, while the flatness does not exhibit a monotonic behaviour, but it is close to 3, as in the case of a Gaussian pdf. Figure 14(b) shows that $\bar{\kappa}_P$ is approximately constant, while rms($\kappa_P$) increases with the increase of rms($T$), even

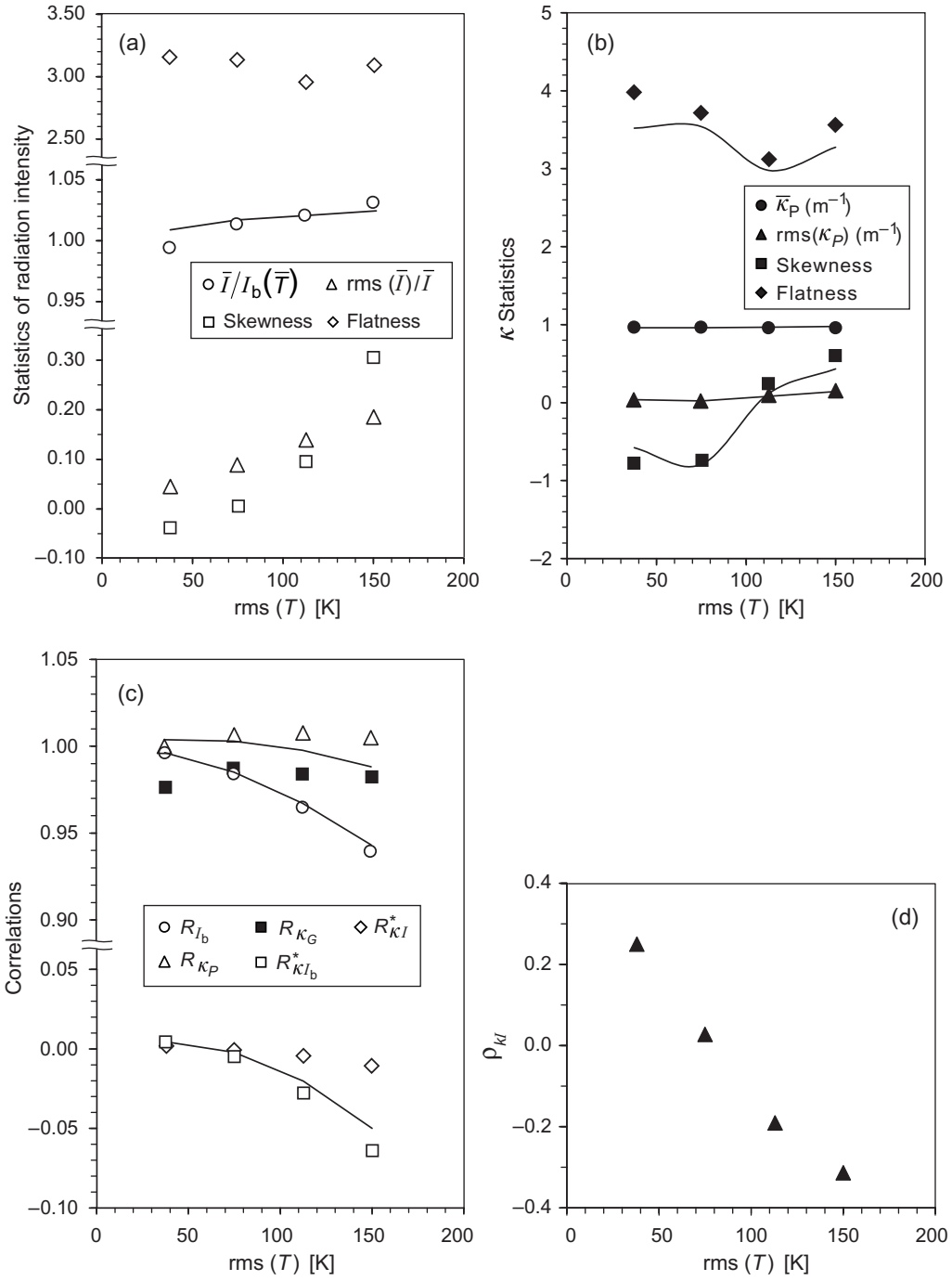


**Figure 14.** Statistics of the radiation intensity as a function of the rms of the temperature of the medium.

though this is hardly visible in the figure. The skewness and flatness of $\kappa_P$ change in a non-monotonic way, which is fairly well reproduced using equations (27) and (28).

The temperature self-correlation becomes more important as the intensity of temperature fluctuations increases, as revealed by $R_{I_b}$ in figure 14(c). The theoretical predictions based on

equation (24) provide excellent agreement. The $\kappa_P$ self-correlation ($R_{\kappa_P}$) is very close to unity, i.e. it plays a negligible role in TRI, while the $\kappa_G$ self-correlation is not so close to unity, but it still is of secondary importance in comparison with $R^*_{kI}$ and $R^*_{kI_b}$. The correlation $R^*_{kI_b}$ increases in absolute value with the increase of rms($T$), and may be predicted with good accuracy using equation (29). The observed trend may be explained using equation (32). In fact, $R_{\kappa_G}/R_{\kappa_P}$ is approximately independent of rms($T$), while $1/R_{I_b}$ increases and $I_b(\bar{T})/\bar{I}$ decreases if rms($T$) increases. However, figures 14(a) and (c) show that the variation of $1/R_{I_b}$ is greater than that of $I_b(\bar{T})/\bar{I}$, and so the second term on the right of equation (32) increases with rms($T$), and it is greater than unity. This explains the evolution of $R^*_{kI_b}$ shown in figure 14(c).

The low values of $R^*_{kI}$ are consistent with the results reported for the previous cases. The increase of $R^*_{kI}$ in absolute value, as a consequence of the increase of the temperature fluctuations, is also consistent with the increase, in absolute value, of the correlation coefficient $\rho_{kI}$, as shown in figures 14(c) and (d).

*3.4.4. Influence of the variance of the molar fraction of $CO_2$.* The influence of the variance of $x_{CO_2}$ is illustrated in figure 15. The mean value of $x_{CO_2}$ was set to 0.1. Hence, for a given instantaneous temperature, the corresponding instantaneous molar fraction of $CO_2$, and therefore the absorption coefficient, which is proportional to $x_{CO_2}$, will be higher than in standard conditions if $T > \bar{T}$ and lower in the opposite case, as concluded from equation (25). This implies that the range of values of radiative emission, in the numerator of equation (24), will be larger than in standard conditions. The mean radiative emission increases with the increase of rms($x_{CO_2}$), because the instantaneous radiative emission at temperatures greater than $\bar{T}$ contribute the most to the mean. The values in the denominator of equation (24) may either increase or decrease, depending on the band and quadrature point under consideration, but the variation of the denominator is smaller than that of the numerator. Therefore, the mean radiation intensity is expected to increase with rms($x_{CO_2}$). The results in [14] and the predictions based on equation (24) confirm this behaviour, which is supported by the DNS data, as shown in figure 15(a). The rms of the radiation intensity remains approximately unchanged, and so do the skewness and the flatness.

Figure 15(b) shows that $\bar{\kappa}_P$ and rms($\kappa_P$) are approximately constant, while the skewness and the flatness change significantly, these changes being rather well predicted by equations (27) and (28). If the scales were enlarged, it could be verified that both $\bar{\kappa}_P$ and rms($\kappa_P$) actually decrease with the increase of rms($x_{CO_2}$). In fact, the increase of rms($x_{CO_2}$) yields a decrease of the range of instantaneous values of $\kappa_P$, and so rms($\kappa_P$) decreases. The corresponding decrease of $\bar{\kappa}_P$ is due to the relatively low values of $\kappa_P$ at both low and high values of $x_{CO_2}$ in comparison with $\bar{x}_{CO_2}$. In the former case, $\kappa_P$ is relatively low because it is proportional to $x_{CO_2}$, and this effect prevails over the temperature dependence, and in the latter case, $\kappa_P$ is relatively low because the temperature is high and overshadows the role of the molar fraction of $x_{CO_2}$, as discussed in [27].

The correlations shown in figure 15 reveal that $R_{I_b}$ does not change with rms($x_{CO_2}$) as expected, since the pdf of temperature remains unchanged. The evolution of $R_{\kappa_P}$ is consistent with that of $\bar{\kappa}_P$, and is qualitatively reproduced using equations (27) and (28). In contrast to the other cases, in the present one $R_{\kappa_P}$ and $R_{\kappa_G}$ exhibit different trends. The reason for this behaviour is not clear. Since both $R_{\kappa_G}/R_{\kappa_P}$ and $I_b(\bar{T})/\bar{I}$ decrease with the increase of the fluctuations of $CO_2$ molar fractions, while $R_{I_b}$ is insensitive to these fluctuations, it follows from equation (32) that $R^*_{kI_b}$ increases, in agreement with the statistical data from DNS. The same trend is followed

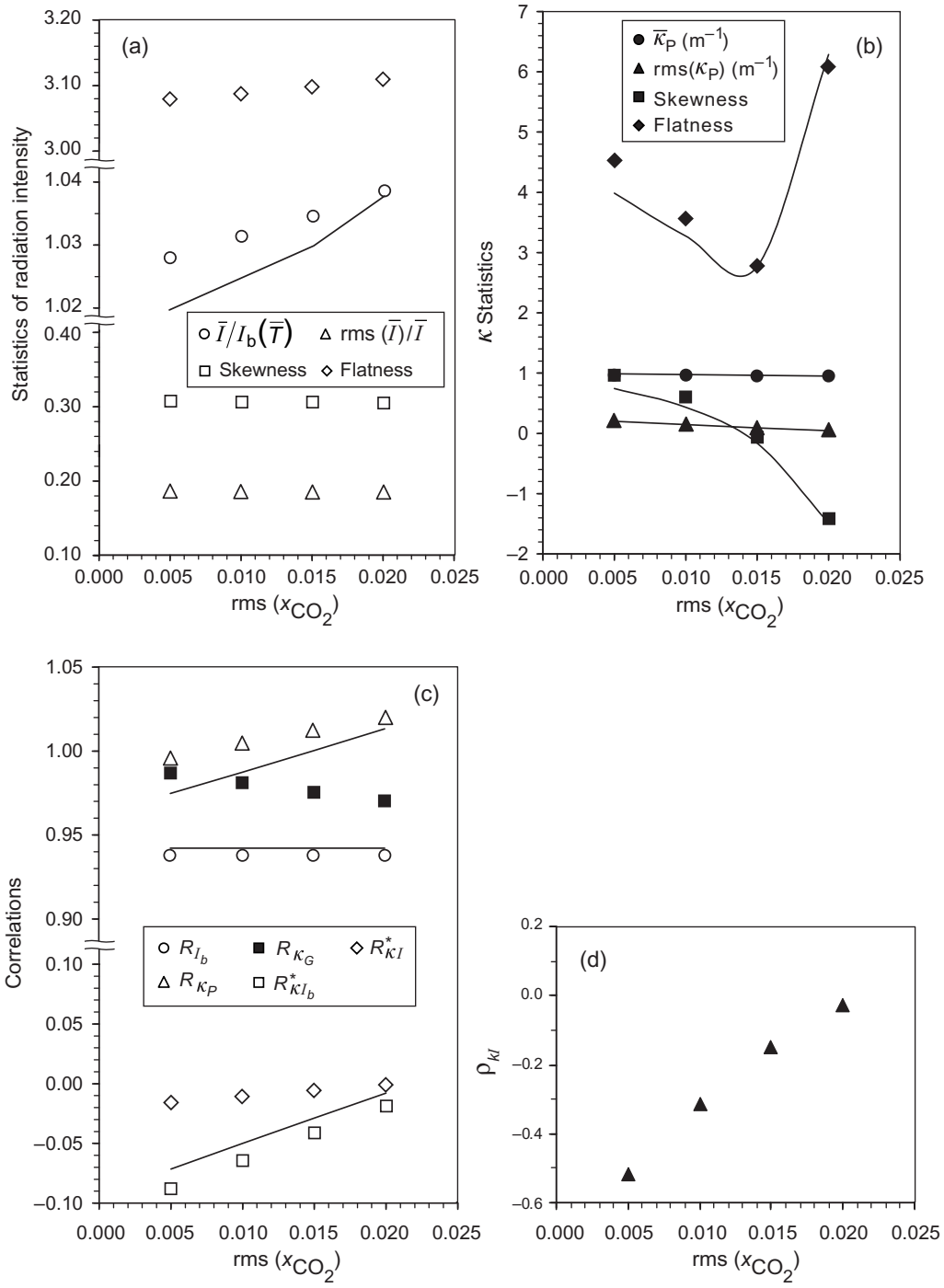


**Figure 15.** Statistics of the radiation intensity as a function of the rms of the molar fraction of $CO_2$.

by $R^*_{kI}$ and $\rho_{kI}$. The values are again close to zero, which supports the OTFA and justifies the good predictions achieved using the time-averaged RTE.

Previous research has shown that TRI is more important in reactive flows than in isothermal flows. Therefore, an important extension of the present work will be the investigation of

radiation statistics for reactive flows. Furthermore, the DNS data may be helpful to evaluate the accuracy of closure models for the emission term of the RTE, which is often based on an assumed shape for the mixture fraction pdf, and to develop a general closure model for the absorption term of the RTE, which is not available at present.

## 4. Conclusions

The interaction between turbulence and radiation in statistically stationary (forced) homogeneous and isotropic turbulence was studied. It was found that about $2 \times 10^5$ samples, corresponding to a single instantaneous field, provide accurate results for the mean and variance of the radiation intensity leaving the domain, but more than 20 instantaneous fields are needed to obtain accurate values for the higher moments of the radiation intensity, as well as a converged pdf of the radiation intensity. In all cases, the correlation between fluctuations of the absorption coefficient and fluctuations of the radiation intensity is small, which supports the optically thin fluctuation approximation, and justifies the good predictions achieved using the time-averaged RTE. The main conclusions drawn from the analysis carried out may be summarized as follows:

1. The radiation intensity is non-Gaussian and is characterized by large structures much larger than the turbulence integral scale. It is not spatially correlated with any of the other turbulence or radiation quantities due to its intrinsic non-local nature. The spectrum of the radiation intensity suggests the existence of a power law close to $-5/2$. This is steeper than the classical $-5/3$ observed in high Reynolds number turbulent jet flames. More work is needed in order to understand the physical processes governing this spectrum and to establish the scaling law for this variable.
2. The mean radiation intensity, normalized by the blackbody radiation intensity at the mean temperature, decreases with the increase of the mean temperature, and increases with the increase on the variance of temperature or variance of the molar fraction of $CO_2$.
3. Turbulence yields an increase of the mean blackbody radiation intensity in comparison with laminar flows, in agreement with past work, and the temperature self-correlation becomes more important whenever the intensity of temperature fluctuations increases.
4. Turbulence generally yields a decrease of the Planck-mean absorption coefficient in comparison with laminar flows for the studied conditions. The Planck-mean absorption coefficient self-correlation is not as important as the temperature self-correlation, i.e. the former is closer to unity. Nevertheless, it was found that the Planck-mean absorption coefficient self-correlation, $R_{\kappa_P}$, decreases with the increase of temperature, is little dependent on the variance of the temperature, and increases with the variance of the molar fraction of the absorbing species.
5. Both $\overline{\kappa'_P I'_b}$ and $\overline{\kappa'_G I'}$ are negative, but the role of TRI is more significant in radiative emission ($\overline{\kappa'_P I'_b}$) than in radiative absorption ($\overline{\kappa'_G I'}$). This supports the OTFA and justifies the good predictions often achieved using the time-averaged RTE. Both $R^*_{kI}$ and $R^*_{kI_b}$ increase, in absolute value, with the variance of the temperature and decrease, in absolute value, with the variance of the molar fraction of the absorbing species.

6. Calculations based on an assumed Gaussian pdf for the temperature yield very good predictions of the mean radiation intensity, temperature self-correlation and moments of the Planck-mean absorption coefficient, particularly the lowest ones. Predictions of the Planck-mean absorption coefficient self-correlation and absorption coefficient-temperature correlation are also fairly satisfactory, and exhibit the correct trends.

Extrapolation of the conclusions of this study to other physical conditions should be cautious, since the practical configurations and conditions may be rather different from the present ones.

## Acknowledgments

This work was developed within the framework of project PPCDT/EME/59879/2004, which is financially supported by FCT-Fundação para a Ciência e a Tecnologia.

## References

[1] Li G and Modest M F 2002 Application of composition PDF methods in the investigation of turbulence-radiation interactions *J. Quant. Spectrosc. Radiat. Transfer* **73** 461–72
[2] Coelho P J 2007 Numerical simulation of the interaction between turbulence and radiation in reactive flows *Prog. Energy Combust. Sci.* **33** 311–83
[3] Kounalakis M E, Gore J P and Faeth G M 1988 Turbulence/radiation interactions in nonpremixed hydrogen/air flames *Proc. Combust. Inst.* **22** 1281–90
[4] Song T H and Viskanta R J 1986 Interaction of radiation with turbulence: application to a combustion system *Thermophys. Heat Transfer* **1** 56–62
[5] Mazumder S and Modest M F 1999 A probability density function approach to modelling turbulence–radiation interactions in nonluminous flames *Int. J. Heat Mass Transfer* **42** 971–91
[6] Li G and Modest M F 2003 Importance of turbulence–radiation interactions in turbulent diffusion jet flames *J. Heat Transfer* **125** 831–8
[7] Coelho P J, Teerling O J and Roekaerts R 2003 Spectral radiative effects and turbulence/radiation interaction in a nonluminous turbulent jet diffusion flame *Combust. Flame* **133** 75–91
[8] Coelho P J 2004 Detailed numerical simulation of radiative transfer in a non-luminous turbulent jet diffusion flame *Combust. Flame* **136** 481–92
[9] Snegirev A Y 2004 Statistical modelling of thermal radiation transfer in buoyant turbulent diffusion flames *Combust. Flame* **136** 51–71
[10] Habibi A, Merci B and Roekaerts D 2007 Turbulence radiation interaction in Reynolds-averaged Navier–Stokes simulations of nonpremixed piloted turbulent laboratory-scale flames *Combust. Flame* **151** 303–20
[11] Kabashnikov V P and Myaskinova G I 1985 Thermal radiation in turbulent flows—temperature and concentration fluctuations *Heat Transfer—Sov. Res.* **17** 116–25
[12] Modest M F and Mehta R S 2006 Modelling absorption TRI in optically thick eddies *Proc. Eurotherm Seminar 78—Computational Thermal Radiation in Participating Media II (Poitiers, France, 5–7 April 2006)* ed D Lemonnier, N Selçuk and P Lybaert (Paris: Lavoisier) pp 63–72
[13] Kounalakis M E, Sivathanu Y R and Faeth G M 1991 Infrared radiation statistics of nonluminous diffusion flames *J. Heat Transfer* **113** 437–45
[14] Kritzstein F and Soufiani A 1993 Infrared gas radiation from a homogeneously turbulent medium *Int. J. Heat Mass Transfer* **36** 1749–62
[15] Chan S H and Pan X C 1997 A general semicausal stochastic model for turbulence/radiation interactions in flames *J. Heat Transfer* **119** 509–16

[16] Poitou D, El Hafi M and Cuenot B 2007 Diagnosis of turbulence–radiation interaction in turbulent flames and implications for modeling in large eddy simulation *Turk. J. Eng. Environ. Sci.* **31** 371–81
[17] Coelho P J 2009 Approximate solutions of the filtered radiative transfer equation in large eddy simulations of turbulent reactive flows *Combust. Flame* **156** 1099–110
[18] Roger M, da Silva C B and Coelho P J 2009 Analysis of the turbulence–radiation interactions for large eddy simulations of turbulent flows *Int. J. Heat Mass Transfer* **52** 2243–54
[19] Jones W P and Paul M C 2005 Combination of DOM with LES in a gas turbine combustor *Int. J. Eng. Sci.* **43** 379–97
[20] dos Santos R G, Lecanu M, Ducruix S, Gicquel O, Iacona E and Veynante D 2008 *Combust. Flame* **152** 387–400
[21] Vincent A and Meneguzzi M 1991 The spatial structure and statistical properties of homogeneous turbulence *J. Fluid Mech.* **225** 1–20
[22] Jimenez J, Wray A A, Saffman P G and Rogallo R S 1993 The structure of intense vorticity in isotropic turbulence *J. Fluid Mech.* **255** 65–90
[23] Girimaji S S and Pope S B 1992 Propagating surfaces in isotropic turbulence *J. Fluid Mech.* **23** 247–77
[24] Soufiani A 1991 Temperature turbulence spectrum for high-temperature radiating gases *J. Thermophys. Heat Transfer* **5** 489–94
[25] Wu Y, Haworth D C, Modest M F and Cuenot B 2005 Direct numerical simulation of turbulence/radiation interaction in premixed combustion systems *Proc. Combust. Inst.* **30** 639–46
[26] Deshmukh K V, Haworth D C and Modest M F 2007 Direct numerical simulation of turbulence–radiation interactions in homogeneous nonpremixed combustion systems *Proc. Combust. Inst.* **31** 1641–8
[27] Deshmukh K V, Haworth D C and Modest M F 2008 Direct numerical simulation of turbulence–radiation interactions in a statistically one-dimensional nonpremixed system *J. Quant. Spectrosc. Radiat. Transfer* **109** 2391–400
[28] da Silva C B, Malico I, Coelho P J and Pereira J C F 2006 An exploratory investigation of radiation statistics in homogeneous isotropic turbulence *Proc. Eurotherm Seminar 78—Computational Thermal Radiation in Participating Media II (Poitiers, France, 5–7 April 2006)* ed D Lemonnier, N Selçuk and P Lybaert (Paris: Lavoisier) pp 215–24
[29] da Silva C B and Pereira J C F 2005 On the local equilibrium of the subgrid-scales: the velocity and scalar fields *Phys. Fluids* **17** 108103
[30] Watanabe T and Gotoh T 2004 Statistics of a passive scalar in homogeneous turbulence *New J. Phys.* **6** 40
[31] da Silva C B and Pereira J C F 2007 Analysis of the gradient diffusion hypothesis in large eddy simulations based on transport equations *Phys. Fluids* **19** 035106
[32] Canuto C, Hussaini M Y, Quarteron A and Zang T A 1988 *Spectral Methods in Fluid Mechanics* (New York: Springer) pp 201–12
[33] Alvelius K 1999 Random forcing of three-dimensional homogeneous turbulence *Phys. Fluids* **11** 1880–9
[34] Pope S 2000 *Turbulent Flows* (Cambridge: Cambridge University Press)
[35] Kuo K K 1986 *Principles of Combustion* (New York: Wiley)
[36] Peters N 1984 Laminar diffusion flamelet models in non-premixed turbulent combustion *Prog. Energy Combust. Sci.* **10** 319–39
[37] Modest M F 2003 *Radiative Heat Transfer* (New York: McGraw-Hill)
[38] Goody R M, West R, Chen L and Chrisp D 1989 The correlated-*k* method for radiation calculations in non-homogeneous atmospheres *J. Quant. Spectrosc. Radiat. Transfer* **42** 539–50
[39] Soufiani A and Taine J 1997 High temperature gas radiative property parameters of statistical narrow-band model for $H_2O$, $CO_2$ and CO, and correlated-*k* model for $H_2O$ and $CO_2$ *Int. J. Heat Mass Transfer* **40** 987–91
[40] Schumacher J, Sreenivasan K R and Yeung P K 2005 Very fine structures in scalar mixing *J. Fluid Mech.* **531** 113–22
[41] Dimotakis P E 2000 The mixing transition in turbulent flow *J. Fluid Mech.* **409** 69–98

[42] Kounalakis M E, Gore J P and Faeth G M 1989 Mean and fluctuating radiation properties of carbon monoxide/air flames *J. Heat Transfer* **111** 1021–30

[43] Zheng Y, Barlow R S and Gore J P 2003 Spectral radiation properties of partially premixed turbulent flames *J. Heat Transfer* **125** 1065–73

[44] Zheng Y and Gore P 2005 Measurements and inverse calculations of spectral radiation intensities of a turbulent ethylene/air jet flame *Proc. Combust. Inst.* **30** 727–34

[45] Watanabe T and Gotoh T 2007 Inertial-range intermittency and accuracy of direct numerical simulation for turbulence and passive scalar turbulence *J. Fluid Mech.* **590** 117–46

[46] Burns S P 1999 Turbulence radiation interaction modelling in hydrocarbon pool fire simulations *Sandia Report SAND99-3190* (Livermore, CA: Sandia National Laboratories)